RP1.4-03

De-risking H_2 Adaptation to Industrial Processes

Final Report

January 2023

Project number:

RP1.4-03

Authors:

Alfonso Chinnici, Adam Gee

Project team:

Alfonso Chinnici, Philip Ingenhoven, Woei Saw, Zhao Tian, Gus Nathan, Paul Medwell – University of Adelaide

Alex Perisa, Owen Lucas – Fyfe

Daniel Krosch – GPA Engineering

David Retallack – FCT Combustion

Ashley Roberts, Carina Pirozzi – Woodside

Owen Sharpe, Aaron Grindlay – AGIG

Yannick Monrolin, Ron Jessen – SA Office of the Technical Regulator

Tristan Bodsworth, Ashima Choudhry – Jemena

Australian Government
Department of Industry, Science, Energy and Resources

Business Cooperative Research Centres Program

This work is funded by the Future Fuels CRC, supported through the Australian Government's Cooperative Research Centres Program. We gratefully acknowledge the cash and in-kind support from all our research, government and industry participants.

IMPORTANT DISCLAIMER

Future Fuels CRC advises that the information contained in this report comprises statements based on research. Future Fuels CRC makes no warranty, express or implied, for the accuracy, completeness or usefulness of such information or represents that its use would not infringe privately owned rights, including any parties intellectual property rights. To the extent permitted by law, Future Fuels CRC (including its employees and Participants) excludes all liability to any person for any consequences, including but not limited to all losses, damages, costs, expenses and any other compensation, arising directly or indirectly from using this report (in part or in whole) and any information or material contained in it.

ACKNOWLEDGEMENT

This work is funded by the Future Fuels CRC, supported through the Australian Governments' Cooperative Research Centres Program. The cash and in-kind support from the industry participants is gratefully acknowledged.

In addition to the named Future Fuels CRC industry partners, valuable contributions were provided by:

- Sreeraj Balachandran and Mike Sisley – Rio Tinto
- Felicity Lloyd – Adbri

PROJECT INFORMATION	
Project number	RP1.4-03
Project title	De-risking Hydrogen Adaptation to Industrial Processes
Research Program	1: Future Fuel Technologies, Systems and Markets
Milestone Report Number	Final Report
Description	This project aims to de-risk the adaptation of renewable hydrogen fuel to thermal industrial processes in which radiation is a dominant heat transfer mechanism, specifically alumina calciners and cement/lime kilns.
Research Provider	The University of Adelaide
Project Leader and Team	Paul Medwell Alfonso Chinnici Philip Ingenhoven Woei Saw Gus Nathan Zhao Tian
Industry Proponent and Advisor Team	Alex Perisa, Owen Lucas – Fyfe Daniel Krosch – GPA Engineering David Retallack – FCT Combustion Ashley Roberts, Carina Pirozzi – Woodside Owen Sharpe, Aaron Grindlay – AGIG Yannick Monrolin, Ron Jessen – SA Office of the Technical Regulator Tristan Bodsworth, Ashima Choudhry – Jemena
Related Commonwealth Schedule	RP1.3.2 Novel concepts and/or prototypes of innovative process technology for future fuels in end-use applications developed. RP1.4.3 Solutions for new/modified industrial equipment delivered to allow for a broader range of fuel compositions.
Project start/completion date	July 2020 / September 2023
IP Status	Confidential
Approved by	Alex Perisa (FYFE)
Date of approval	20 January 2023

Table of Contents

SUMMARY OF REPORT

This document represents a consolidated report summarising the key outcomes from all activities carried out within the Future Fuels CRC RP1.4-03 project. In particular, the key results from a joint techno-economic (TEA), process modelling and computational fluid dynamics (CFD) analysis on the effect of blending up to 25% by volume hydrogen with natural gas into the fuel stream on Australian alumina and integrated cement sectors. In addition, experimental data around probing the efficacy of doping biofuels into blended natural gas / hydrogen flames as an adaptation strategy to enhance visibility and radiant fraction of hydrogen-based flames are also reported and discussed.

For the alumina sector, the emissions reduction potential via hydrogen (H_2) blending up to 25% by volume into natural gas was found to be significant in absolute terms, by up to 0.9 $MtCO_{2\text{-}e}$ per year, although its relative impact is relatively low at approximately 6% of the total sector's CO_2 emissions. In a scenario of 25% H_2 blending by volume, some 0.12 Mt of low-carbon H_2 per year—corresponding to half of Australia's H_2 production in 2020—would be needed to satisfy this energy requirement for the alumina sector. This amount of H_2 blending is expected to have negligible impact on the sale price of the alumina. For integrated cement plants, the economic benefit for H_2 blending is less significant compared with that of alumina production. The estimated emissions reduction potential associated with H_2 blending (up to 25 vol.% H_2) was found to be fifty times less in absolute terms than for alumina (up to 0.02 $MtCO_{2\text{-}e}$ per year), and also an order of magnitude less in relative terms (only 0.39% of the total sector CO_2 emissions, due to the majority of the emissions being derived from the limestone itself) and because the natural gas to be replaced with H_2 only accounts for 20% of the total energy consumed by sector (with coal still being the predominant fuel). This indicates that the cement sector is not likely to benefit significantly from a H_2 blending strategy in terms of decarbonisation. The TEA suggests that blending is likely to be economically feasible for the case of alumina production even though, for both the alumina and cement sectors, the parity cost for H_2 to displace natural gas (NG) is around 1–2 A$/kg for a NG price of 9–18 A$/GJ. That is, an economic gap still exists against the projected prices for H_2 delivered via a pipeline in Australia by 2030 and 2050. Carbon taxes could help reducing this gap although very high taxes (150 to 230 A$/ton$CO_2$, depending on NG cost) would be required to achieve a zero gap by 2030. Nevertheless, regardless of the likely economic gap between parity and predicted H_2 prices, the TEA revealed that the estimated increase in the final cost of the two commodities due to H_2 blending is very small at only 0.01–3% depending on NG price and H_2 blending level. This small increase is unlikely to impact significantly on the sale price because it is negligible when compared with the commodity's price fluctuations due to supply/demand changes. Furthermore, this slight increase is likely to be more than offset by the marketing advantage, which highlights that the alumina sector can likely benefit from adopting an H_2 blending strategy in the short term. The process modelling of the last step of the alumina Bayer process also demonstrates that this step can be undertaken with H_2 blends (up to 25 vol.% H_2) with negligible changes on product quality and process performance, and with no modification to current operations and plant layout needed (other than changes to plant equipment to accommodate H_2 in the valves and flowmeters).

The CFD analysis of a simplified NG-fired rotary kiln burner configuration identified that hydrogen blending by up to 10% H_2 by volume will introduce only relatively small changes to the flame and burner performance. On the other hand, for the 25% H_2 blending scenario, a significant increase in NO_x emissions (70% increase in comparison with the baseline case being NG-only) was found to be likely, indicating that appropriate NO_x control strategies would likely be needed to accommodate this level of H_2 blending. The analysis also showed that burner modifications are likely to be able to overcome this increase. For example, reducing the primary air ratio was found to significantly reduce the NO_x emissions for the H_2 blended fuel for the burner configuration assessed here. Nevertheless, these details are all configuration specific, so would need to be optimised on a case-by-case basis.

The experimental analysis on the impact of adding toluene (as representative of a biofuel) as a dopant to 100% H_2 and blended H_2/NG flames to increase both visibility and radiant fraction from flames revealed that while this strategy can significantly improve these two key factors of H_2-based flames at laboratory scale, 4% by vol. of toluene would be required for 100% H_2 flame to achieve similar characteristics to that of pure NG flame. That is, 65% by mass and 40% by energy input of toluene will be needed to achieve same performance as per NG flames, indicating that the amount of doping fuel required is too great for any practical use. A basic techno-economic analysis also revealed that with current and predicted prices of NG, H_2 and biofuels, this adaptation strategy is very costly, suggesting that alternative strategies should be developed and assessed.

1. INTRODUCTION

This final report consolidates the key outcomes from the Future Fuels CRC RP1.4.03 activities regarding de-risking hydrogen (H_2) adaptation into industrial process, with a key focus on the Australian alumina and integrated cement sectors. Natural gas (NG) in Australia provides 25% of all energy produced annually, and in 2015-16 more than 30 Mt was utilised across all sectors. Industrial use (excluding electricity), accounts for more than 30% of NG consumption, which has seen a steady 2% increase on a 10-year average [1]. The project is focussed on investigating the strategies and knowledge required to displace NG with H_2, particularly by de-risking H_2 adaptation into those industrial processes in which radiation is a dominant (and/or a contributing) heat transfer mechanism. The alumina sector is the single largest industrial consumer of natural gas (NG) in Australia with 150 PJ of NG consumed per year on average [2]. The current annual production of metallurgical alumina is 21 million tonnes (Mtpa) [3,4], making the sector Australia's largest high temperature mineral processing industry, generating more than $7 billion in revenue from export alone [5] and making Australia the second largest global exporter of this commodity. The NG is consumed at six sites in WA and QLD, with approximately one third consumed in the last, high temperature step of the so-called Bayer process, where gibbsite, $Al(OH)_3$, is converted to Smelter Grade Alumina (SGA) by heating it to temperatures of around 1000°C. The calcination step involves the release of chemically bound water during heating, followed by the material undergoing phase transformations, and the remaining two thirds consumed in the initial low and mid- temperature steps for the digestion process [3]. The total greenhouse gas (GHG) emissions from Australia's alumina refineries are presently 15 Mt of $CO_{2\text{-}e}$ per annum, corresponding to 24% of Australia's Scope 1 manufacturing carbon emissions. Of this, over 60% can be directly attributed to NG utilisation, which is the main energy source driving the different processes [3]. Therefore, it is essential to identify appropriate strategies to reduce the NG-dependency and associated emissions for the Australian alumina sector, which will also support the global decarbonisation effort in reaching net-zero targets by 2050. Hydrogen (H_2) blending with NG into pipelines has been anticipated as being a potential transition decarbonisation strategy, before a second stage conversion towards 100% H_2 [6]. However, the impact of H_2 blending on potential reduction of CO_2 emissions, appliance performance and final cost of alumina needs to be carefully assessed as a function of blending ratio and fuel cost to inform decision makers and relevant industry players on the benefits, effectiveness and challenges associated with adopting a blending strategy as a short- to mid-term decarbonisation approach.

The Australian integrated cement production sector consumes 5 PJ per annum of NG [7]. This corresponds to 20% of the total energy consumption for this sector, with coal still being the dominant energy source [7]. Currently, Australian cement production is approximately 10 Mtpa, all being used for the domestic market. The total GHG emissions from Australia's integrated cement plants are 5 Mt of $CO_{2\text{-}e}$ per annum, of which 60% are attributed to the process (anthropogenic emissions associated with limestone calcination) and the remaining 40% to fuel utilisation [7]. Given the relatively low consumption of NG for the integrated cement sector (in comparison with the alumina sector), the high reliance on coal, and the emissions primary being associated with the process itself rather than from burning a fuel, it can be anticipated that the H_2 blending strategy would also have commensurately less impact on decarbonisation of the sector. Nevertheless, it remains important to quantify to what extent this sector could benefit from adopting a H_2 blending strategy while obtaining a high-level understanding of its potential efficacy as a decarbonisation tool. In addition, given that the presence of H_2 in H_2/CH_4 blends could potentially impact both NO_x emissions and radiation heat transfer rates [8] in rotary kilns, with radiation representing the main heat transfer mechanism, there is also a need to systematically assess the impact of H_2 blending on appliance performance to identify any issues with compatibility. This knowledge is also needed to inform both the gas producers and the end users on the limits, potential impediments (e.g., potential drastic changes in performance) and opportunities of H_2 blending while also generating new knowledge needed to assist regulators with the certification of these appliances.

A key fundamental challenge in H_2 fuel utilisation is the reduced visibility and radiant heat transfer efficiency as a result of displaced carbon in the fuel. While low-carbon fuel is a viable option to reduce CO_2 emissions, a consequence of this is reduced soot formation [9]. In hydrocarbon-based fuels, the major contributor to radiative heat transfer is the re-radiating of thermal energy from soot particles. The 'glowing' of heated soot particles is also the source of the yellow colour of a rich hydrocarbon flame. The notion to increase soot formation is counterintuitive

from a health and environmental standpoint, and certainly soot poses a risk in those areas, but its contribution to combustion performance and process efficiency is critical and cannot be ignored. Combustion applications which rely on radiant heating as their primary mode heat transfer will require a solution to operate successfully on large fractions of hydrogen. Recent research has investigated the use of flame dopants to increase the radiant heating capacity of low-sooting flames. The concept of adding pulverised coal or non-reacting nanoparticles has been considered as a means of mimicking the effects of soot [10]. Most recently the use of bio-oils has been proposed as a means of increasing soot loading in poorly radiating flames [11]. Nevertheless, there is still limited data and understanding of bio-fuel doping on combustion characteristics of H_2-based flames, so that there is a need for a systematic assessment of this adaptation strategy.

In light of the aforementioned needs and gaps, this consolidated report summarises the key outcomes from all the Future Fuels CRC RP1.4.03 activities regarding de-risking hydrogen adaptation into industrial process. A combination of different tools, namely computational fluid dynamics (CFD) and process modelling, and experimentation were used to assess the impact of H_2 blending (into NG), on performance of selected appliances/flames and processes (alumina calcination) as well as on key techno-economic indicators and emissions reduction potential. The key results from the following activities are reported and discussed herein:

- first-order techno-economic (TEA) modelling assessing the impact of H_2 blending (up to 25% by vol.) on emission reduction potential, H_2 and NG requirement, H_2 parity cost, and final cost of commodities, for the Australian alumina and integrated cement sectors.
- process modelling of the impact of H_2 blending (up to 25% by vol.) on performance and operation of an alumina gas suspension calciner.
- CFD modelling of a simplified NG-fired rotary kiln and a commercial NG-fired straight-grate iron ore pelletiser to assess the impact of H_2 blending (up to 25% by vol.) on flame and burner performance.
- experimental investigation of using bio-oil doping as a potential strategy to increase the radiant heat transfer and visibility of H_2 (100%) and blended H_2/CH_4 flames.

2. TECHNO-ECONOMIC ANALYSIS

2.1 MODEL DESCRIPTION

The TEA model is a first-order, input–output, energy-based model, requiring data input from the literature about total commodity production cost, total fuel (NG) consumption, GHG emissions, cost breakdown for the final commodity, and energy consumption by fuel source for each sector to obtain output data. The H_2 blending ratio was varied over the range 0–25% by volume while the NG fuel cost was varied over the range 3–25 A$/GJ. It is assumed that the H_2 is introducing into all the combustion appliances needed for the Bayer process, including both appliances for low and mid-temperature steps of the process (e.g., turbine, boilers) as well high temperature calciners. A detailed study on H_2 adaptation into the last step of the Bayer process (calciner) is discussed in Section 3. The NG-only case was considered as the reference case, with 9 A$/GJ being the reference NG price, and 450 and 135 A$/tonne being the reference final prices for alumina and cement, respectively, following both the 2020 Australian Aluminium Council and Cement Industry Federation reports [3,7]. For selected cases, the impact of introducing a carbon tax on output data variation was also assessed. Figure 1 illustrates the overall structure of the TEA model.

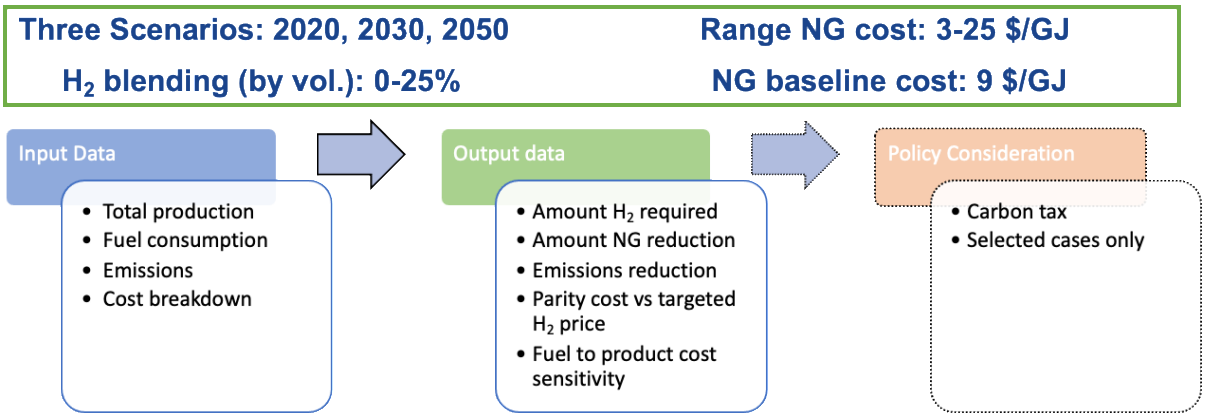

Figure 1: Technoeconomic analysis (TEA) modelling approach for both alumina and integrated cement sectors.

An extensive literature review was carried out to obtain the input data required for the TEA model for both alumina and integrated cement sectors. Figure 2 presents the industry-averaged values of total current energy consumption by energy source for the two sectors in 2020 while the total commodity production, energy consumption (absolute and by tonne of product), and associated GHG emissions can be found in Milestone 4 Report of this project [12].

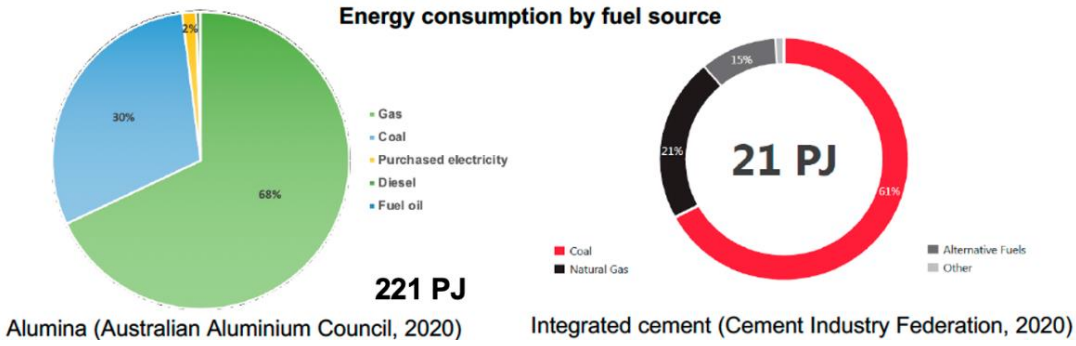

Figure 2: Australia's nationally averaged energy consumption by fuel source in 2020 for both the alumina and integrated cement production sectors. Data taken from Australian Aluminium Council 2020 report and Cement Industry Federation 2020 report [3,7].

To evaluate the hydrogen parity cost with NG, the economic gap for the different scenarios and impact on final cost of commodities, both the cost breakdown for the commodity cost as well as the predicted cost of H_2 price are required. Figure 3 presents the cost breakdown for alumina and cement (on average in Australia), while Table 1 reports the predicted cost of H_2 delivered to the Australian pipeline, estimated by Worley Advisian [13], for the different time horizons and production technologies (electrolytic and steam methane reforming with carbon capture).

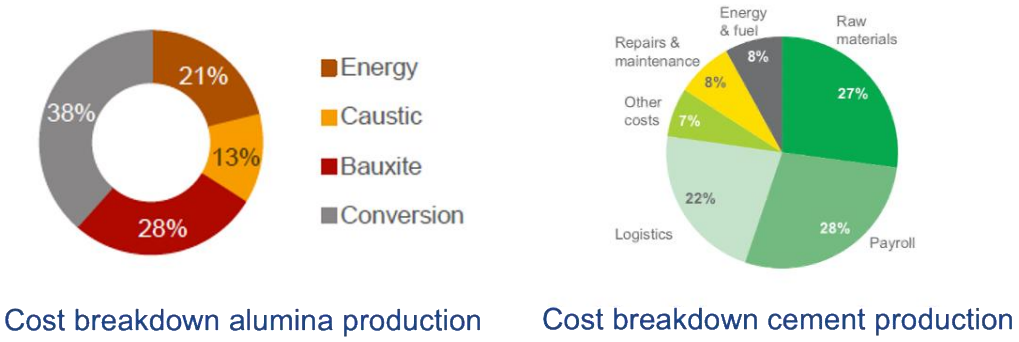

Figure 3: Cost breakdown for commodity production. Data taken from the Alumina Limited 2020 report and 2020 Results report (Boral) [14,15]. Conversion in cost breakdown of alumina production includes employee costs, indirect costs and other raw material costs.

Table 1: Estimated cost of H_2 delivered to Australian pipeline for different hydrogen production routes and time horizons. Data taken from Worley Advisian 2021 report [13].

Year	Electrolytic H_2 A$/kg	H_2 from NG (SMR +CCUS) A$/kg
2020	3.3 – 4.6	2.86 – 3.95
2030	2.3 – 3.4	2.6 – 3.5
2050	1.5 – 2.6	2.6 – 3.6

All the key model equations for the different scenarios and fuel price sensitivity can be found in Milestone 4 Report of the project [12].

2.2 KEY RESULTS: ALUMINA SECTOR

Figure 4 presents the Mtpa of H_2 and NG required to satisfy the current energy demand (from NG) for the alumina sector for a ratio of H_2 blending in the range 0–25% by volume. Figure 4 indicates that 0.04 $Mtpa_{H2}$ and 0.12 $Mtpa_{H2}$ would be required for the 10% and 25% H_2 blending scenarios, respectively. Production of H_2 in Australia was 0.25 Mtpa in 2020 (mainly used in petrochemical refineries, [17]), thus the demand would be 17% and 50% of total H_2 produced in Australia to satisfy H_2 blending demand from the alumina refineries, although it would need to be provided by new capacity of green/blue hydrogen to be an environmental benefit. To put this in perspective, the supply of 0.12 Mtpa from an electrolysis plant would require its capacity to be approximately 700 MW_e. This represents a seventy-fold scale-up from the 10 MW units presently being supported by ARENA for construction in Australia. Hence this demand would greatly accelerate the establishment of a domestic H_2 supply chain. Alternatively, it would be sufficiently large scale to justify the construction of a blue-hydrogen production facility. Figure 4 also shows that the amount of NG required as a function of the H_2 blending level exhibits a linear relation, with up to 10% savings in NG consumption for the 25% H_2 blending scenario (from 3.33 Mt of NG for the baseline case down to 3 Mt).

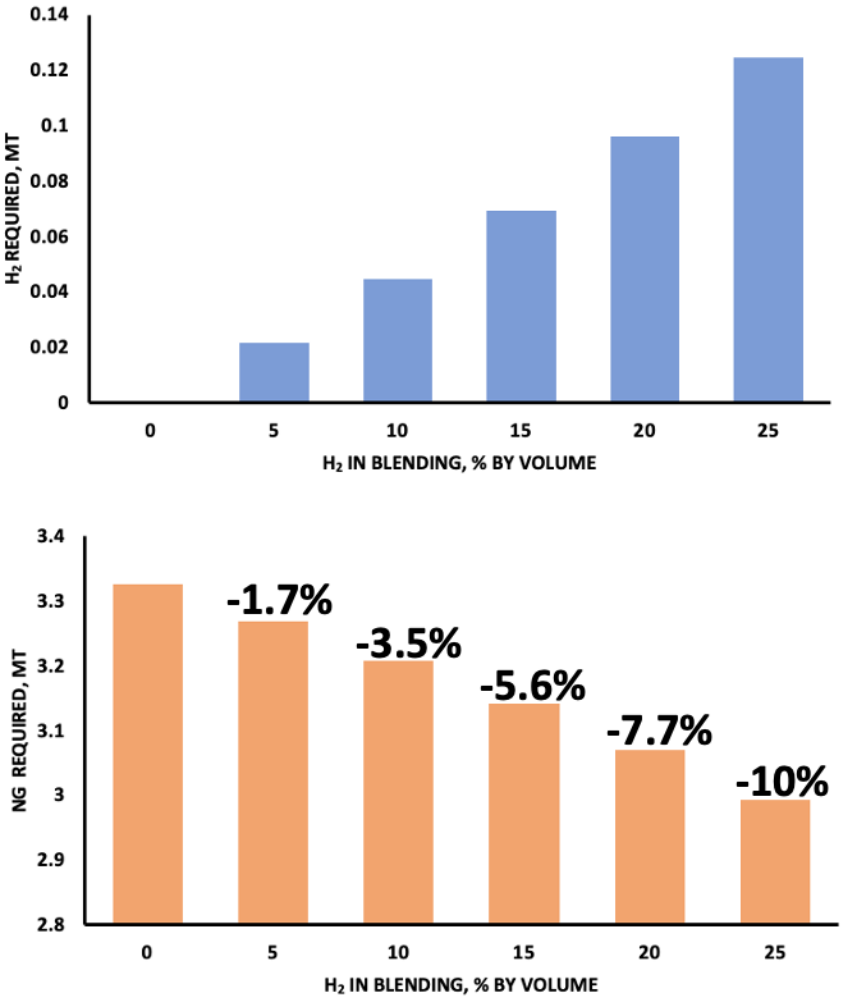

Figure 4: Amount of H_2 required (in Mt) to satisfy the current energy demand (from NG) for the alumina sector for a level of H_2 blending in the range 0–25% by volume.

Figure 5 presents the emissions from Australia's alumina plants (both in absolute values and as a percentage) as a function of H_2 blending ratio. Both the electrolysis and SMR+CCUS low-carbon H_2 cases are shown. It can be seen that up to 0.88 $CO_{2\text{-}e}$ Mt per year can be avoided for a 25% H_2 blending scenario when H_2 is supplied to the pipeline. This corresponds to approximately 6% of the total sector $CO_{2\text{-}e}$ emissions (14.9 Mt in 2020) and to 10% of the emissions associated with NG consumption (9.8 Mt in 2020). That is, a moderate carbon emission avoidance via H_2 blending is potentially possible from such a blending approach. Also, note that the use of SMR+CCUS low-carbon H_2 (here a 90% capture efficiency is considered) leads to much lower $CO_{2\text{-}e}$ emissions avoidance in comparison with electrolytic H_2 (-1.4 and -4% reduction against baseline NG-only case for 10 and 25% H_2 level, respectively) mainly due to indirect emissions.

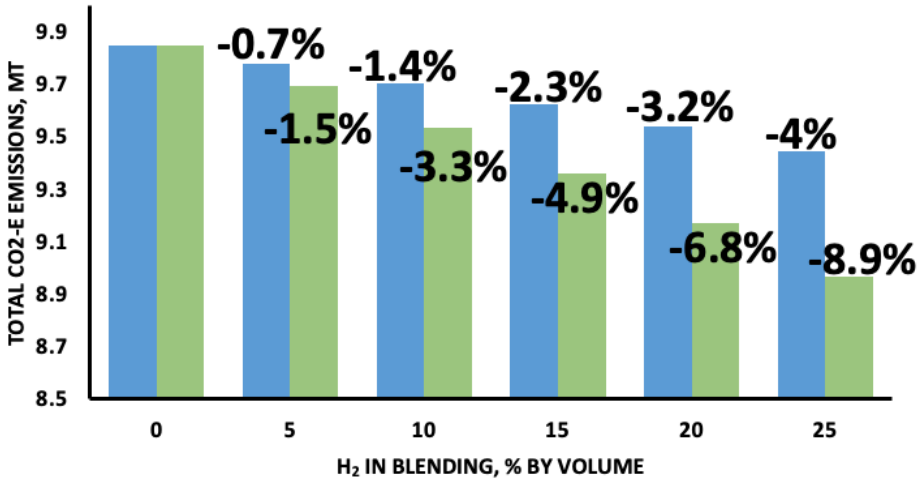

Figure 5: The CO_2 emissions (per year) from Australia's alumina plants as a function of the hydrogen blending ratio in the fuel. Electrolytic H_2 = green bar, SMR-CCUS low-carbon H_2 = blue bar.

Figure 6 presents the alumina cost sensitivity as function of the NG price for the baseline NG-only case (plus the percentage difference against the reference value of A$9/GJ), and the calculated H_2 parity cost with NG for two level of H_2 blending.

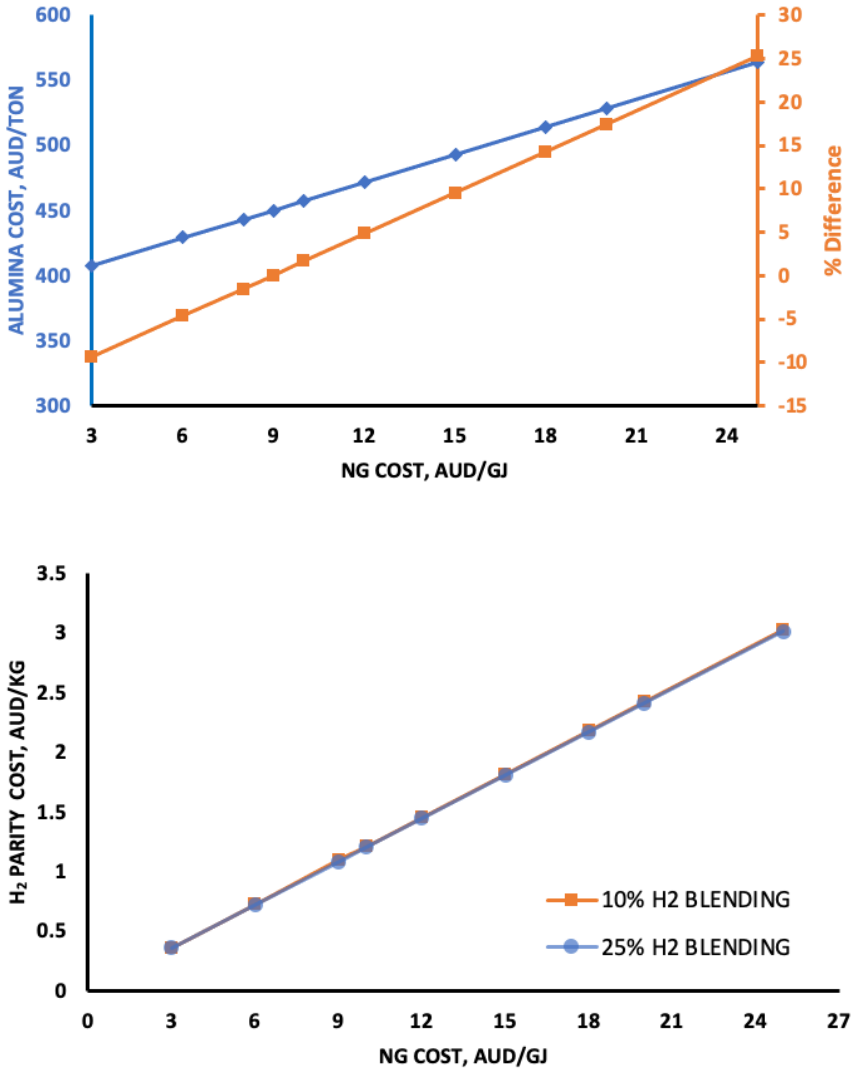

Figure 6: The sensitivity of the cost of alumina production on the NG price for the baseline NG-only case, shown in absolute and relative terms, for the reference price of A$9/GJ – top figure. The lower figure presents the calculated H_2 parity cost to displace NG for two level of H_2 blending.

From Figure 6 it can be seen that, in the NG-only case, an increase of the NG price from 9 to either 18 or 25 A$/GJ would increase the final alumina cost by 15 and 25%, respectively (while keeping all the other cost components fixed). This because of the high share % of NG on the final cost of alumina. Overall, compared with the reference NG price of A$9/GJ, the alumina price would vary in the range -10 to +25%, for a NG price in the range 3–25 A$/GJ. It can also be seen that the level of H_2 blending has not an influence on the H_2 parity cost with NG, and that for a NG price of A$9/GJ, the parity with NG for alumina production requires an H_2 price of around A$1/kg. This value approximately doubles to A$2.2/kg for a NG price = A$18/GJ.

Figure 7 presents the economic gap between the calculated values of H_2 parity cost with NG reported in Figure 6 and the average values of the predicted H_2 price (delivered to pipeline) reported in Table 1, for a 10% H_2 blending by volume, and for both electrolytic and SMR+CCUS low-carbon H_2. The trends highlight that an economic gap

exists between cost parity and predicted H_2 prices, with this gap still significant during the period to 2050. The analysis also estimates the values of the NG price needed to achieve a zero economic gap for all the scenarios (i.e., H_2 parity cost = H_2 predicted delivered costs), which are showed in Figure 8. It can be seen that the required cost of NG to achieve no economic gap would be 27–33, 22–25 and 16–25 A$/GJ for 2020-, 2030- and 2050-time horizons, respectively.

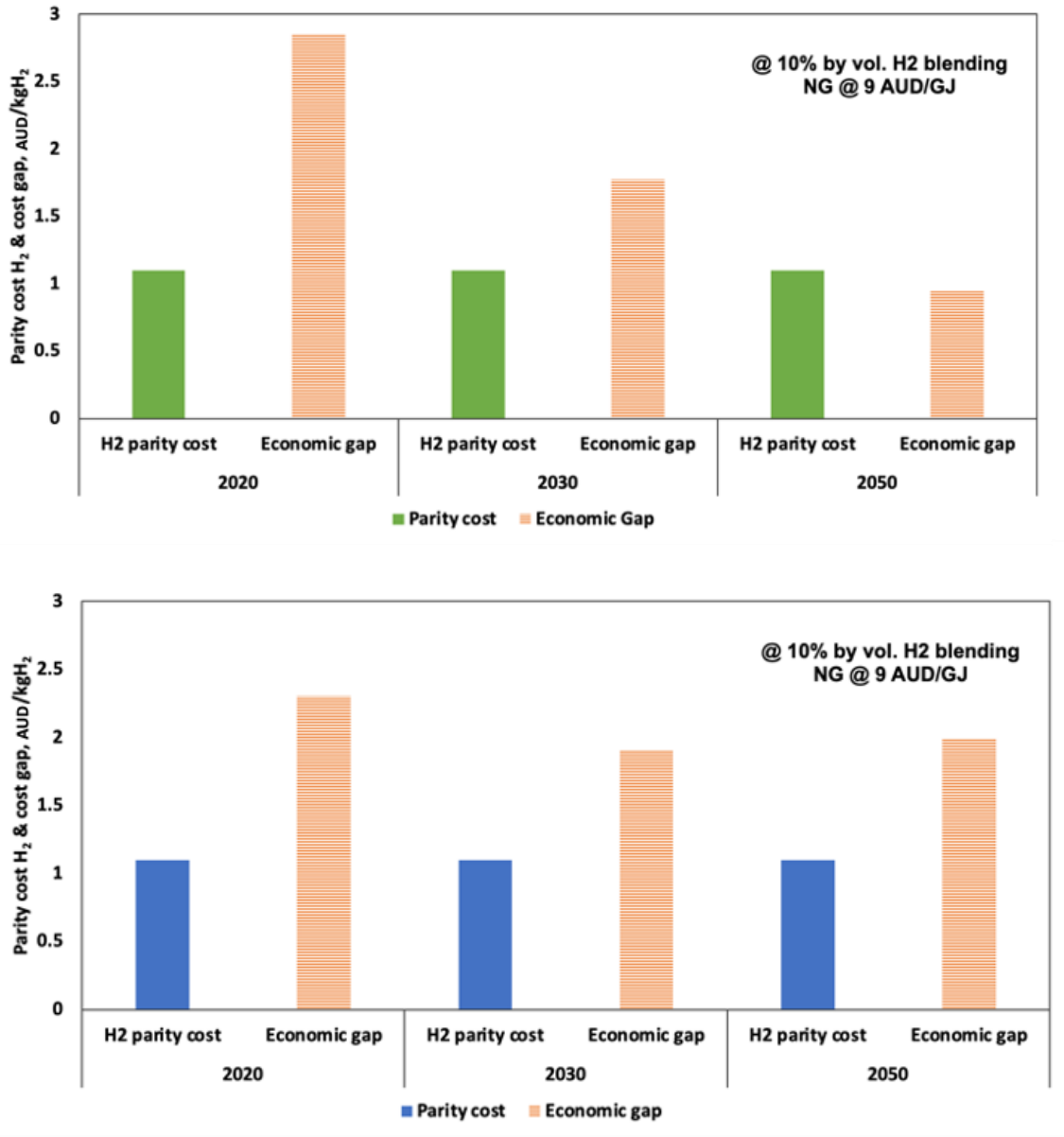

Figure 7: The calculated economic gap between the hydrogen cost delivered to pipeline (present and projected) and the calculated H_2 parity cost with NG, for the cases of green hydrogen (top) and blue hydrogen (bottom). The average values of the predicted H_2 price (delivered to pipeline) are based on data reported in Table 1, for a 10% H_2 blending by volume, and for both electrolytic (top) and SMR+CCUS low-carbon H_2 (bottom).

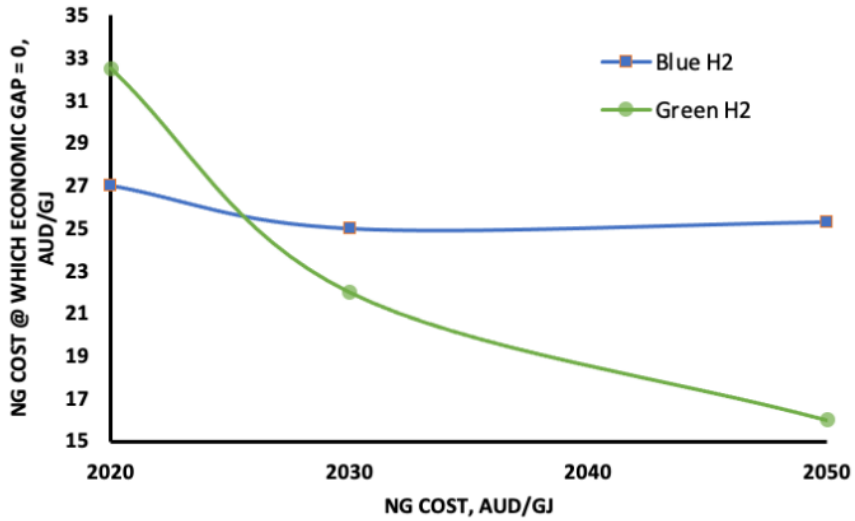

Figure 8: Cost of NG at which economic gap between parity and predicted prices of H_2 is zero, for both electrolytic and SMR-CCUS low-carbon H_2 (labelled green and blue in the legend, respectively), for a 10% H_2 blending by volume.

Figure 9 shows that the introduction of a carbon tax would reduce the economic gap between NG-only and H_2 blending. It can be seen that low to very high carbon taxes will be required to meet predicted H_2 costs by 2030 and 2050. In particular, in the 2030 transition scenario, a tax of 150–230 A$/ton$CO_2$ will need to be introduced to achieve a zero economic gap, for a 10% H_2 blending scenario, and a NG price in the range 9–15 A$/GJ. To put this in perspective, the Grattan Institute predicts the adoption of a 35 A$/ton$CO_2$ carbon tax in Australia by 2030 [18]. Hence, mechanisms such as a carbon tax would help in reducing the economic gap but are unlikely to have a significant impact with current predicted tax values. It is worth noting that very similar trends were obtained for a 25% H_2 blending scenario (not shown for brevity).

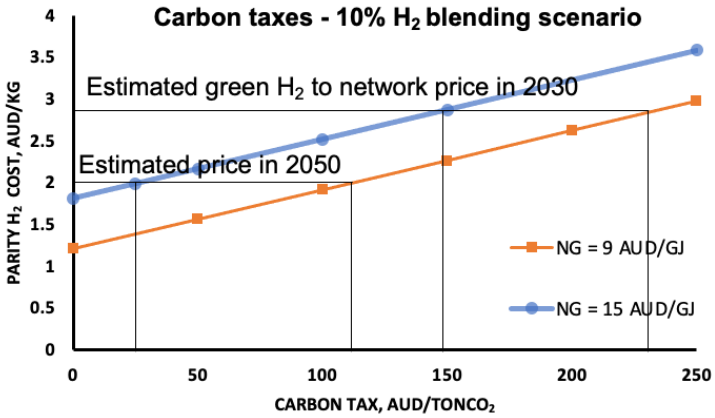

Figure 9: Value of carbon tax required to achieve a zero economic gap between the parity and projected H_2 costs by 2030 and 2050 for green H_2 scenarios presented in Table 2, for a 10% H_2 blending by volume, and for two prices of NG (9 and 15 A$/GJ).

Finally, Figure 10 presents the impact of switching to H_2 for different scenarios (10–50% H_2 blending by volume using projected 2030 costs for H_2 from electrolysis) and the corresponding cost increase as a percentage against the NG-only case (note that the cases for 50% H_2 by volume is only reported for completeness, but do not account for any cost increase arising from major CAPEX changes that would be required to infrastructure). Also shown is the world alumina production, consumption and price changes due to supply/demand [19]. It can be seen that, although a zero economic gap between H_2 parity cost with NG and predicted H_2 cost is unlikely to be achieved by 2030, the increase in alumina price due to H_2 blending, is only 0.01–3% in comparison with the NG-only baseline case, depending on NG price and H_2 blending level. This because 10–25% H_2 by volume is only 1.4–4% by mass. This increase is also much lower than the predicted increase in the alumina cost if NG was to vary from 9 to 12 A$/GJ for the NG-only case. To note that the predicted price increase due to H_2 blending is negligible when compared with the alumina price fluctuations due to supply/demand changes, indicating that the adaptation of an H_2 blending strategy can be seen as a very promising transition pathway to decarbonise the alumina sector. The trends reported in Figure 10 highlight that even in scenarios featuring an economic gap between H_2 parity with NG and predicted H_2 cost, the impact of switching to H_2 blending on the final product cost is very small, and negligible in some cases.

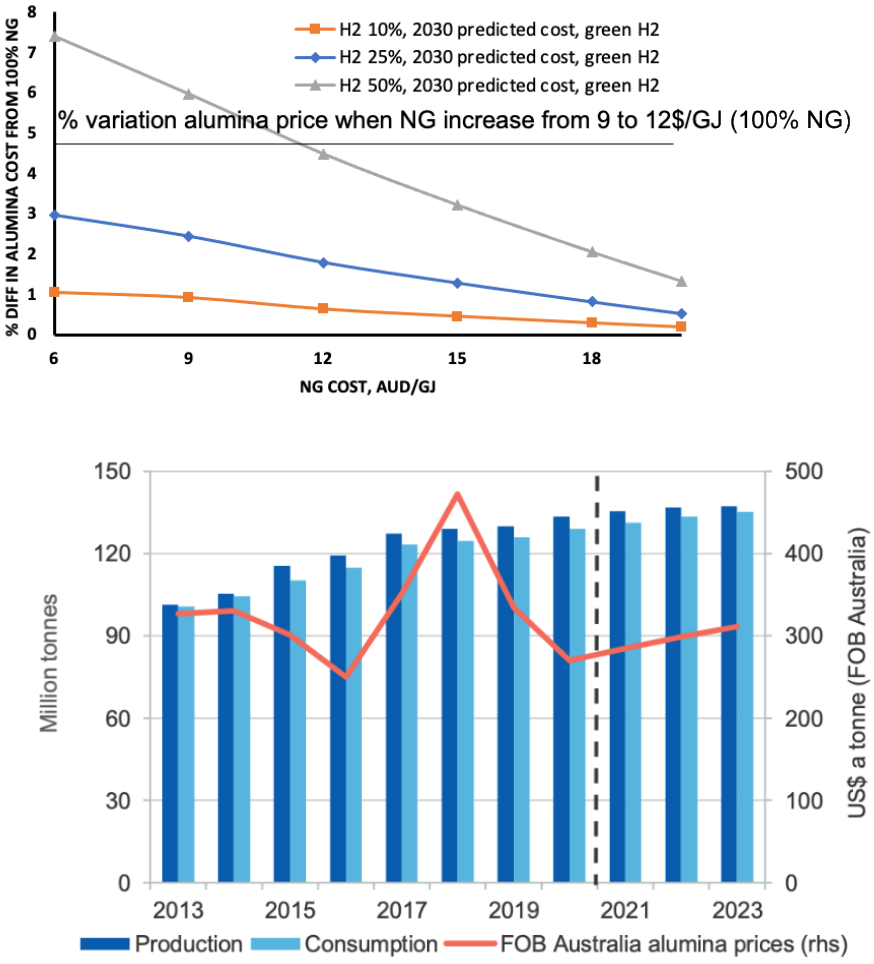

Figure 10: Cost increase as a percentage of the final alumina price for different scenarios against the NG-only case for 10–50% H_2 blending by volume using predicted 2030 electrolytic H_2 cost. Also shown is the world alumina production, consumption and price changes due to supply/demand [19]. Note that the case for 50% H_2 by volume is only reported for completeness but do not account for any major CAPEX changes that would be required to infrastructure.

2.3 KEY RESULTS: INTEGRATED CEMENT SECTOR

Figure 11 presents the calculated amount of H_2 and NG (in Mt) required per year as well as corresponding total $CO_{2\text{-}e}$ emissions, for the different H_2 blending considered here. It can be seen that only 0.00125 and 0.0033 Mt per annum of H_2 are needed to satisfy the energy demand in the 10% and 25% H_2 blending scenarios, respectively. These values represent 0.5 and 1.3% of current Australian H_2 production and are one order of magnitude lower than the corresponding H_2 demand for the alumina sector for the same levels of H_2 blending. Up to 10% of NG consumption can be avoided in the 25% H_2 blending scenario (i.e., 10% savings), although the absolute value of avoided NG consumption (being only 0.009 Mt per annum of NG) is relatively small in comparison with that of the alumina sector. The estimated emissions reduction potential associated with H_2 blending (up to 25% H_2 by vol.) was found to be negligible (up to 0.02 $MtCO_{2\text{-}e}$ per year, i.e., only 1% of the equivalent emissions associated with fuel, and 0.39% of the total sector emissions) regardless of the H_2 production route considered, which indicates that this sector is not likely to significantly benefit from an H_2 blending strategy in terms of decarbonisation in the short term. This is primarily because the majority (60% of the total) of the sector CO_2 emissions are linked to the process rather than the fuel, and secondarily because NG only accounts for 20% of the total energy consumed the sector (with coal still being the predominant fuel source).

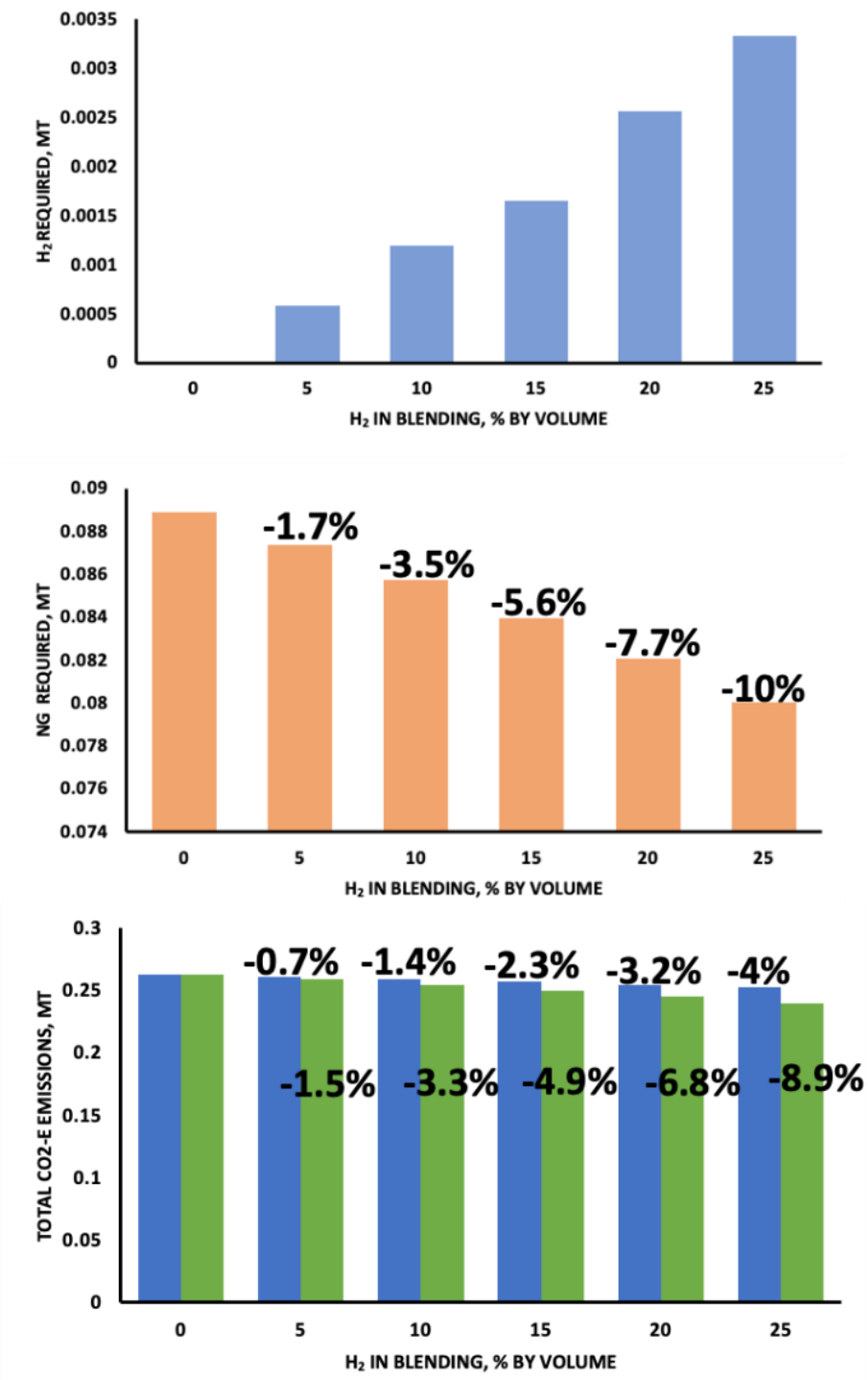

Figure 11: Amount of (top) H_2 and (mid) NG required for the different H_2 blending ratio (per year), and (bottom) corresponding total $CO_{2\text{-}e}$ emissions for electrolytic and SMR-CCUS low-carbon H2 routes. Electrolytic H_2 = green bar, SMR-CCUS low-carbon H_2 = blue bar.

Figure 12 presents the calculated H_2 parity cost with NG as well as the impact of H_2 blending on final cost of cement (both absolute value and relative change in comparison with the NG-only case reported here) for different NG price and H_2 blending levels. It can be seen that the trends are similar to those reported in Figure 6. That is, parity with NG for cement production will require an H_2 price delivered to the pipeline of around 1.1 and 2.2. A$/kg, assuming NG at 9 and 18 A$/GJ, respectively. Also, the predicted increase in the final cost of cement due to H_2 blending switching is negligible (<0.5% in comparison with the baseline NG-only case) for a blending level of up to 25% by volume, and by assuming the 2030 electrolytic H_2 price delivered to pipeline (A$2.85/kg, see Table 1).

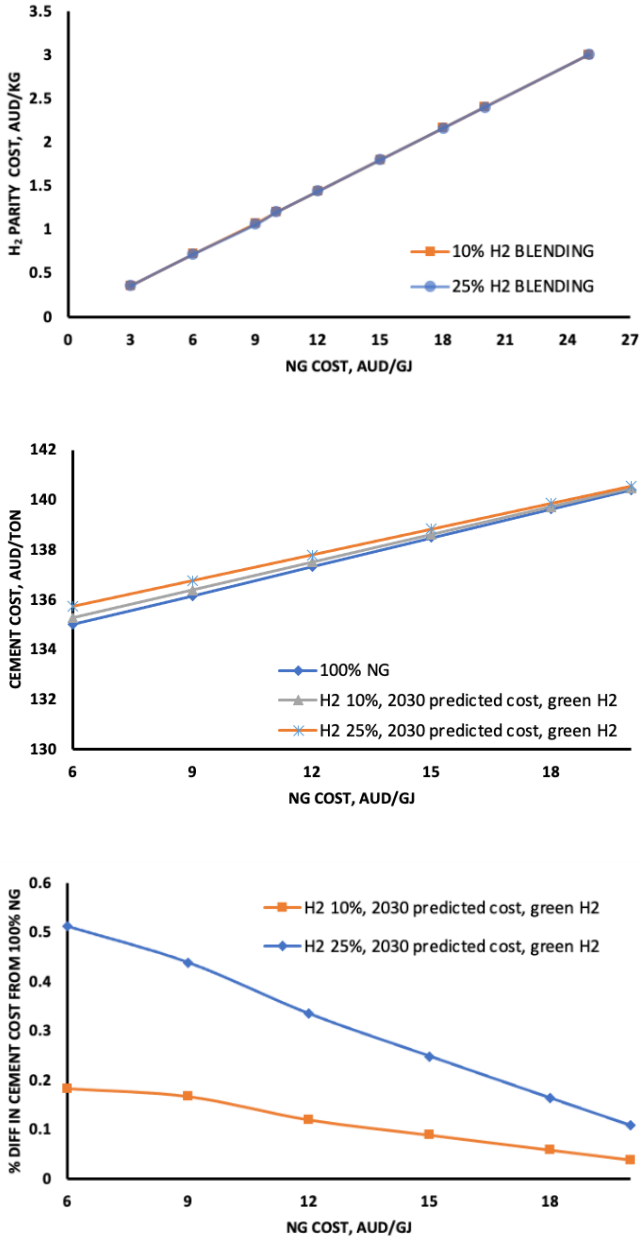

Figure 12: Calculated cost of H_2 parity with NG and impact of H_2 blending on final cost of cement (absolute value and relative change relatively to NG-only case), for different NG price and H_2 blending levels.

3. PROCESS MODELLING

3.1 DESCRIPTION OF ASPEN MODEL

A process model was developed using Aspen Plus v11 software package to assess the impact of H_2 blending on performance of a NG-fired alumina calciner. Figure 13 presents a schematic diagram of the gas suspension calcination process, where gibbsite particles are calcined into smelter grade alumina (SGA). Fine gibbsite particles (100–150µm) with surface moisture of approximately 5–9%, are preheated and partially calcined with hot flue gas exiting the holding vessel, through a two-stage cyclone (P01 and P02). Here, the cyclones are assumed to have a solid recovery of 95% and to operate as counter-current heat transfer units, in which the particles and gases enter at different temperatures but reach the same temperature at the outlet. The four-stage cooling cyclone system (C01 to C04) is used to cool the alumina particles whilst preheating the fresh air that is required for the combustion in the main furnace. The alumina particles are further cooled down to 60 °C using a fluidised bed cooler. The fine particles in the flue gas after P01 are removed using an electrostatic precipitator (ESP) before the flue gas, whose temperature is that for water condensation (~140°C), is vented to the atmosphere. The Aspen+ software is used to perform a mass and energy balance for each unit operation based on each individual chemical species entering and exiting each individual unit operation as shown in Figure 14. The model was verified against existing, available data to prove reliability/confidence with prediction prior to perform a sensitivity on H_2 blending ratio. For all cases, the input fuel is adjusted to maintain a constant value of thermal energy input, while the input air mass flow was kept constant to ensure minimal changes to the alumina cooling and preheating systems. This approach requires no changes to be made to the fan setting on the alumina cooling/air preheating side, which ensures that this part of the process is not affected by any variations in fuel mixture, and a minor variation on the equivalence ratio (from 0.85 with NG-only down to 0.83 for NG/H_2 with 25% H_2 by vol.).

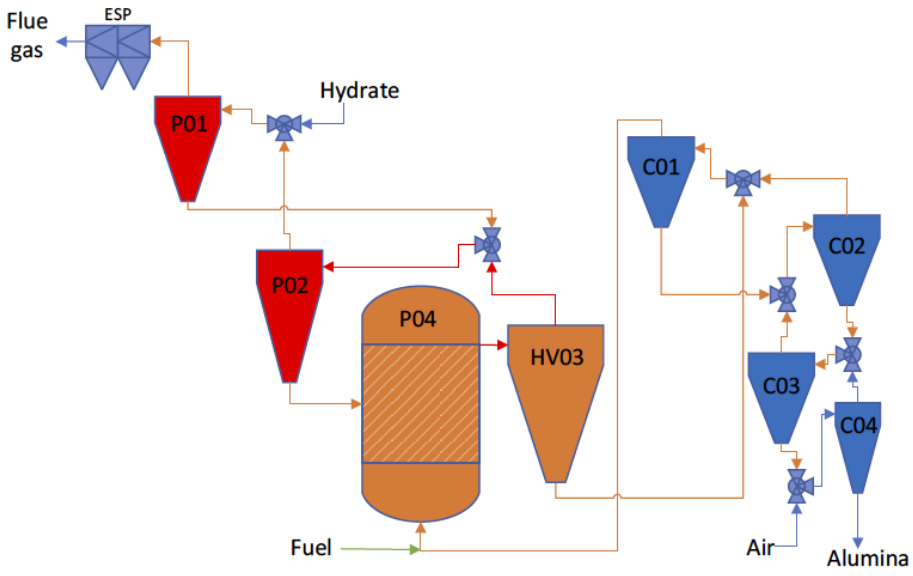

Figure 13: Gas Suspension Calciner (GSC flow sheet) of the model. Cyclone P01 (red) is the drier, Cyclone P02 (red) is the pre-calciner, P04 (orange) is the main calciner, HV03 (orange) in the holding vessel, while Cyclones C01-C04 (blue) are used to achieve the cooling and heat recovery.

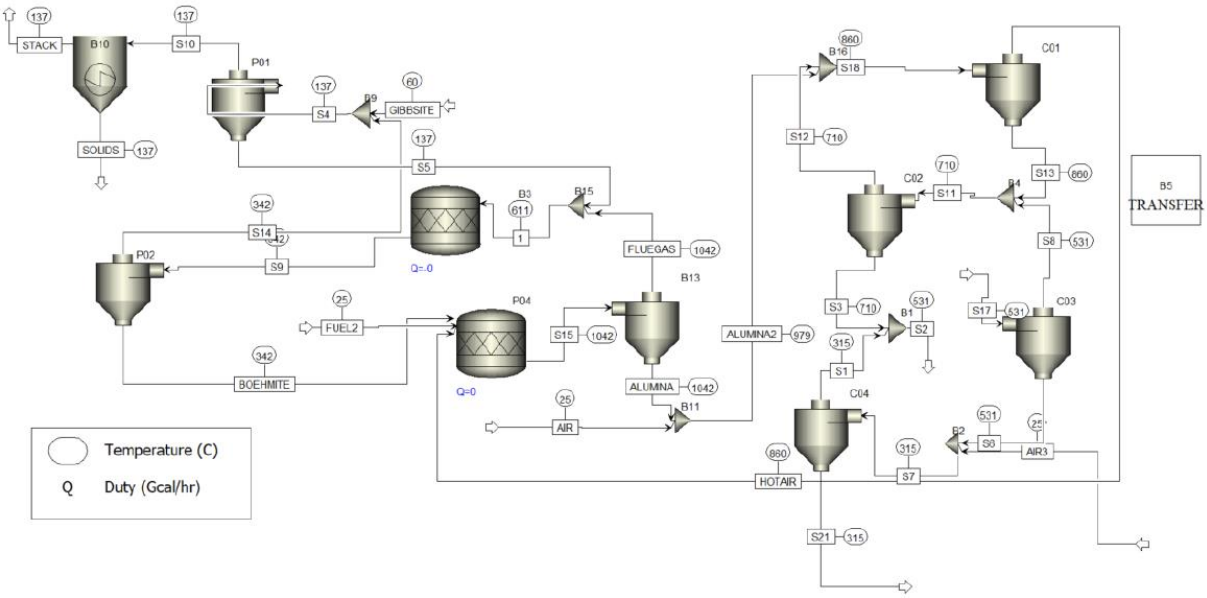

Figure 14: Process flow diagram developed in Aspen+ to model a gas suspension calciner.

3.3 KEY RESULTS

Table 2 summarises the relative changes for the relevant system parameters as a function of H_2 blending. The total volumetric flow rate of fuel input can be seen to increase by up to 21%. However, as the fuel only constitutes about 10% of the total inlet gas flow rate, the total volumetric flow rate of gases is increased by only 2% for the highest H_2 blending ratio considered here. The reduction in CO_2 and natural gas usage, calculated with the Aspen model are between 1.6 and 9.1%, while the water content in the flue gas is below 1% for all the blending ratios investigated. Note that the changes are reported in percentage terms, and are assumed independent of the exact physical dimensions of the calciner. The overall changes to the alumina output are minimal for all analysed blending ratios.

Table 2: Relative changes of fuels and total gas flow rates, as well as those for velocity and residence time, as calculated with the Aspen model for a series of hydrogen blending ratios in natural gas.

H_2 in natural gas (vol%)	0%	5%	10%	25%
Fuel volumetric flow-rate increase	0%	4%	7%	21%
Total inlet volumetric flowrates change	0%	0%	1%	2%
Inlet velocity changes within ducts and the calciner	0%	0%	1%	2%
Residence time changes	0%	0%	1%	2%
H_2O output in flue gas [wt.%]	0%	0.2%	0.3%	0.9%
CO_2 emissions reduction [wt.%]	0%	-1.6%	-3.3%	-9.1%
CH_4 reduction [wt.%]	0%	-1.6%	-3.3%	-9.1%

Tables 3–6 present the detailed results for the main calciner for the inlet and outlet streams. The main calciner has three inlet streams, namely, the solid inlet stream from the pre-calciner, the air inlet stream and the fuel inlet. The solids inlet stream consists of the pre-calcined raw material, boehmite and alumina, neither of which change significantly when the blending ratio is varied. Similarly, the temperature with which these materials exit the pre-calciner, does not change significantly.

Table 3: Solid inlet stream to the main calciner from the pre-calciner system as calculated with the Aspen model for a series of hydrogen methane blending ratios.

Blending Ratio	0%	5%	10%	25%
Temperature [°C]	342	342	342	342
Boehmite [kg/hr]	138,800	138,800	138,800	138,800
Alumina [kg/hr]	10,030	10,020	10,020	10,000

Table 4: Air inlet stream from the heat recovery system as calculated with the Aspen model for a series of hydrogen methane blending ratios.

Blending Ratio	0%	5%	10%	25%
Temperature [°C]	861	861	859	859
N_2 [kg/hr]	93,400	93,400	93,400	93,400
O_2 [kg/hr]	28,380	28,380	28,380	28,380
Alumina [kg/hr]	9,468	9,469	9,471	9,472

Materials exits the main calciner in two ways, with the solids mainly being collected in the holding vessel (Table 5). The output remains approximately unchanged when the blending ratio is changed. The temperature changes only very slightly, assuring that product quality is not affected by the slight differences in conditions for the different cases. The dusty gas exiting the main calciner is fed back into the pre-calciner where it is used to recover the dust and provide energy for the pre-calcination (Table 6).

Table 5: Solid outlet stream from the main calciner (P04) / holding vessel (HV03).

Blending Ratio	0%	5%	10%	25%
Temperature [°C]	1,043	1,042	1,041	1,040
Alumina kg/hr]	127,300	127,300	127,400	127,400

Table 6: Flue gas outlet stream from the main calciner (P04)/holding vessel (HV03).

Blending Ratio	0%	5%	10%	25%
Alumina [kg/hr]	10,070	10,070	10,060	10,050
N_2 [kg/hr]	93,400	93,400	93,400	93,400
O_2 [kg/hr]	4,447	4,520	4,582	4,824
H_2O [kg/hr]	34,310	34,440	34,600	35,120
CO_2 [kg/hr]	16,460	16,200	15,930	14,960

The particle size distribution and mass density at the calciner outlet were also analysed. The values of d_{80}, d_{50} and d_{10} of the particle size distribution are reported in Table 7. No changes were found for d_{50} and d_{10} and mass density, while changes in d_{80} were minimal when the H_2 blending ratio was varied in the range 0–25% by vol.

Table 7: Particle size distribution and mass density at calciner outlet (S15)

Blending Ratio	0%	5%	10%	25%
d_{80} [particle size in m]	1.18×10^{-5}	1.22×10^{-5}	1.22×10^{-5}	1.22×10^{-5}
d_{50} [particle size in m]	8.0×10^{-6}	8.0×10^{-6}	8.0×10^{-6}	8.0×10^{-6}
d_{10} [particle size in m]	2.0×10^{-6}	2.0×10^{-6}	2.0×10^{-6}	2.0×10^{-6}
Mass density at calciner outlet [kg/m^3]	0.454	0.454	0.454	0.454

4. CFD ANALYSIS

4.1 ROTARY KILN: MODEL DESCRIPTION AND KEY RESULTS

A literature review of available industrial burner designs and data for NG-fired rotary kilns highlighted that, while some data are available for coal-fired kilns, information regarding design and performance of industrial scale NG-fired kilns is limited. In particular, insufficient data are available that are suitable for the development and reliable validation of numerical models. On this basis, the NG-fired kiln configuration selected here to perform a sensitivity analysis of the impact of H_2 blending on flame characteristics is that provided by the KAUST group in Saudi Arabia, a simplified configuration [20-22]. This was selected because, although it reports a simplified kiln design, the burner retains the key features of those encountered in industrial kilns (including swirl and secondary air preheating) and sufficient information is available to allow a CFD model to be developed and validated for this kiln. Figure 15 presents the physical model schematic of the KAUST kiln and a 2D sketch of the computational domain. It can be seen that the kiln input features three streams, namely fuel, primary air (not preheated), and a preheated secondary air stream. The burner is a co-annular swirl burner type with the fuel entering the kiln via the central nozzle, and the primary combustion air entering the kiln via the annulus with a swirl motion. The secondary air is not swirled. The diameter of the fuel nozzle, d_0, is 50 mm, the primary to fuel diameter ratio, d_p/d_0, is 2.3, the kiln diameter is 2.6 m, and its length is 20 m. The baseline case considers NG as the only fuel, adiabatic walls, a fixed thermal input of 2 MW, a value of the primary air ratio (by mass), α, of 10%, no swirl, an air-to-fuel equivalence ratio, λ, of 1.3 (Φ=0.77), and a temperature of the secondary air stream of 1000 °C. The primary air is unheated.

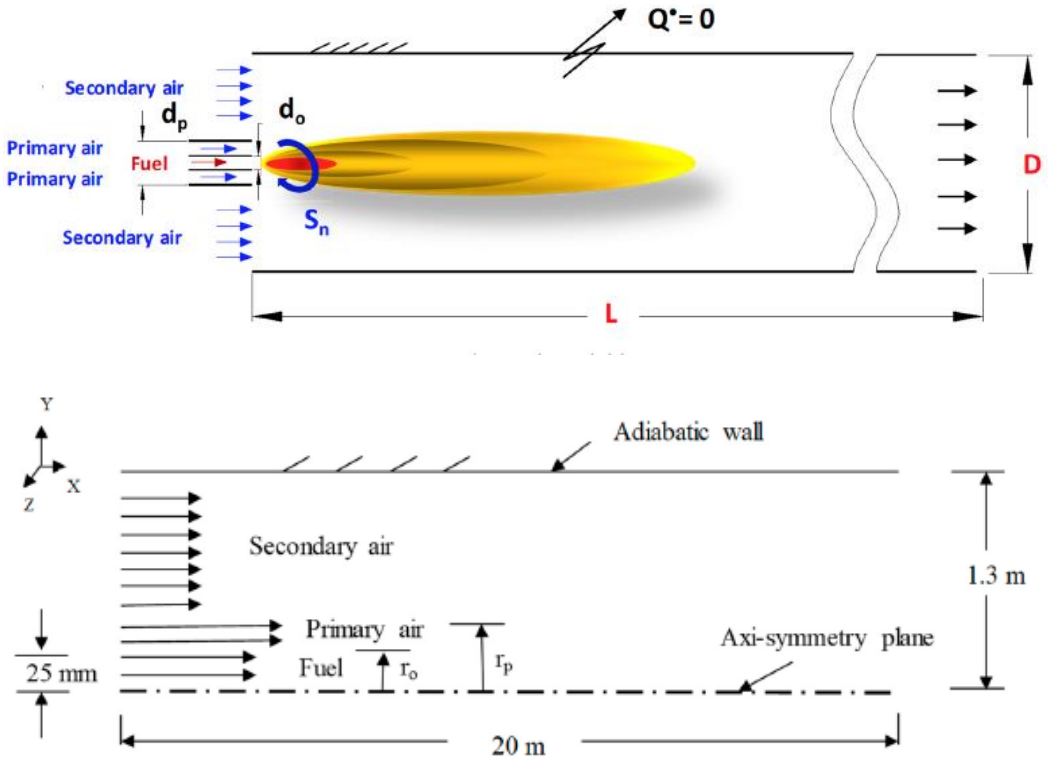

Figure 15: (top) Physical model schematic of the simplified KAUST NG-fired rotary kiln, and (bottom) a 2D sketch of the computational domain [20-22].

A two-dimensional CFD model of the KAUST kiln was developed in ANSYS FLUENT 2021 (R2). To reduce the computational cost of each simulation, only half of the kiln was considered here (i.e., an axisymmetric kiln was modelled), following previous works [20-22]. A structured mesh (quadrilateral cells) was used here to perform a

sensitivity analysis. Mesh independence and mesh quality were checked to ensure its suitability. In particular, mesh quality was checked for skewness, aspect ratio, orthogonality and expansion factor. A total of approximately 120k cells was employed here for all cases investigated (mesh independence was checked against 60 and 250k cells). To note, a 3D model of the domain (a quarter of it) was also developed to evaluate the suitability of a 2D simulation. The difference in the overall flame features between 2D and 3D simulations were less than 5%, indicating that a 2D simulation would provide sufficient accuracy in reproducing flame characteristics for the selected burner. Similar considerations have also been reported previously [20-22].

For all simulations, the k-ε realisable model was selected as the turbulence closure model. The Discrete Ordinates (DO) method was selected to describe the radiative equation and the weighted-sum-of-gray gases model (WSGGM) was used to calculate the spectral properties. The SIMPLE algorithm was employed for pressure-velocity coupling. The Eddy Dissipation Concept with a semi-detailed chemistry (the DRM-19 mechanism, consisting of 19 species and 84 reactions was employed here) was selected to describe the turbulence-chemistry interaction. NO_x emissions were calculated in post-processing. All the key NO_x formation/destruction mechanisms were included in the model, particularly thermal, prompt, N_2O and re-burning mechanism. Due to lack of experimental data, a full validation of the model developed here was not possible. Nevertheless, the model setup is the same of some of our previous numerical works on CH_4, CH_4/H_2 and 100% H_2 flames [23-25]. In particular, in these works, the CFD models were fully validated against available experimental data both at laboratory and pilot scale with a high level of accuracy, hence providing confidence of the reliability of the model developed here. In particular, the model setup was extensively validated/used by our group for modelling non-premixed swirl flames (e.g., TECFLAM burner, [22]), partially premixed and fully premixed swirl flames (e.g., IFRF, UoA burners, [23-25]). The models were able to predict macro features of these flames including peak temperature and thermal profiles, heat transfer rates and radiative component as well as pollutant emissions.

The matrix of investigation for all the cases investigated here is reported in Table 8. The main parameters that were varied in the sensitivity analysis were the H_2 blending ratio, the vane angle of the primary air stream (with 0 representing the no swirl case) and the value of the primary air ratio (by mass). Both adiabatic and non-adiabatic wall boundary conditions were considered for the kiln walls. Adiabatic simulations were carried out to assess the effect of H_2 blending on flame characteristics, while heat flux profiles and radiant contribution were obtained from non-adiabatic simulations. It is worth noting that, for α =10%, the Craya-Curtet parameter [26], *CC*, which is a key parameter for confined turbulent jets systems like those encountered in a confined rotary kiln environment, was calculated to be approximately 2 for both CH_4-only and CH_4/H_2 cases. This value of *CC* ensures an appropriate level of recirculation in a kiln (a value of $CC > 1.5$ is required for recirculation to occur), and it is in line with the values at which industrial kilns typically operate ($1.5 < CC < 2.5$) [21].

Table 8: Matrix of investigation for the CFD sensitivity analysis.

H_2 in fuel stream, (vol.%).	**Swirl Vane Angle (°)**	**Primary air ratio, α (%)**	**Preheating Temperature (°C)**	**Wall BC**
0, 5, 10, 15, 20, 25	0,15,30,45,60	3, 10	1000	Adiabatic, 5% heat losses

Figure 16 presents the calculated 2D kiln temperature contour for the NG-only case, and a comparison of the centreline temperature profile along the kiln axis as a function of the H_2 blending ratio, and for a fixed primary air ratio (α = 10%) and secondary preheating temperature (1000 °C). The cases reported here are for a non-swirled primary air stream. It can be seen that the structure, and macro features of NG and NG/H_2 flames analysed here are similar to each other, for the range of H_2 blending considered here.

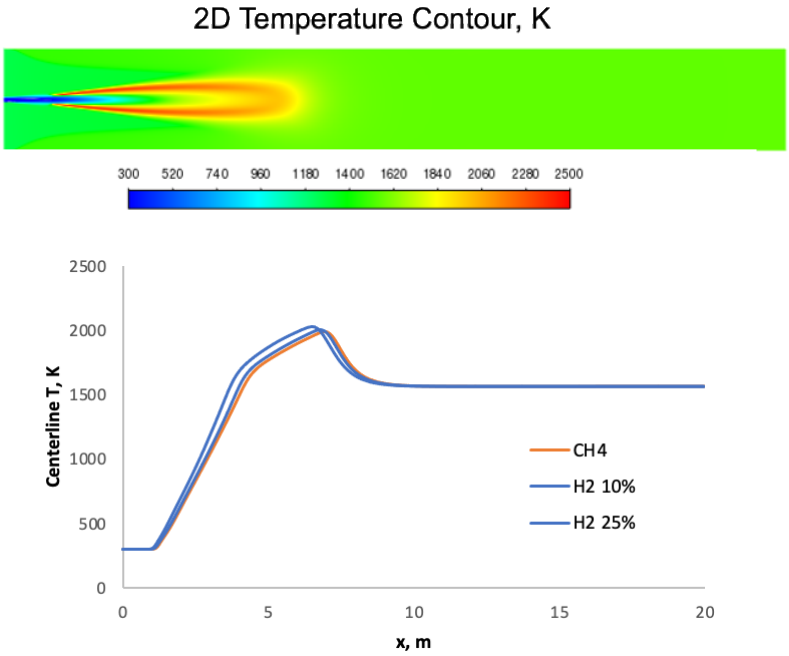

Figure 16: (top) Cross-sectional distribution of temperature for the NG-only case, and (bottom) centreline temperature profile along the kiln axis as a function of H_2 blending level, and for a fixed primary air ratio (10%) and secondary preheating temperature (1000 °C). The cases reported are for a non-swirled primary air stream.

Figures 17 presents the calculated peak flame temperature, flame length and NO_x emissions as a function of the H_2 blending ratio, for a fixed primary air ratio (α = 10%) and secondary air preheating temperature (1000 °C), and for a non-swirl primary air stream. Both the absolute values and relative differences in comparison with the baseline NG-only case are shown. It can be seen that the addition of H_2 to the CH_4 fuel stream leads to only a small change to the peak temperature and flame length (corresponding with the position of the centreline peak temperature in this analysis) for all the range of H_2 blending considered here. In particular, an increase in H_2 blending of up to 25% by volume, was found to decrease the flame length by 6% in comparison with the NG-only case, and a peak flame temperature increase 50 K. This is in line with the higher reactivity and adiabatic flame temperature of H_2 relative to NG. On the other hand, while the NO_x emissions were found to increase slightly for the 10% H_2 blending case in comparison with the NG-only baseline case (by 12%), a significant impact on NO_x emissions is predicted for the 25% H_2 blending case (70% increase). Note that similar trends and observations were found also for the cases with swirled primary air (Figure 18), indicating that this sharp increase in NO_x emissions is to be attributed solely to H_2 switching. This increase is likely attributable, in part, to the thermal NO_x mechanism, owing to the higher temperature. This is in line with previous observations [27].

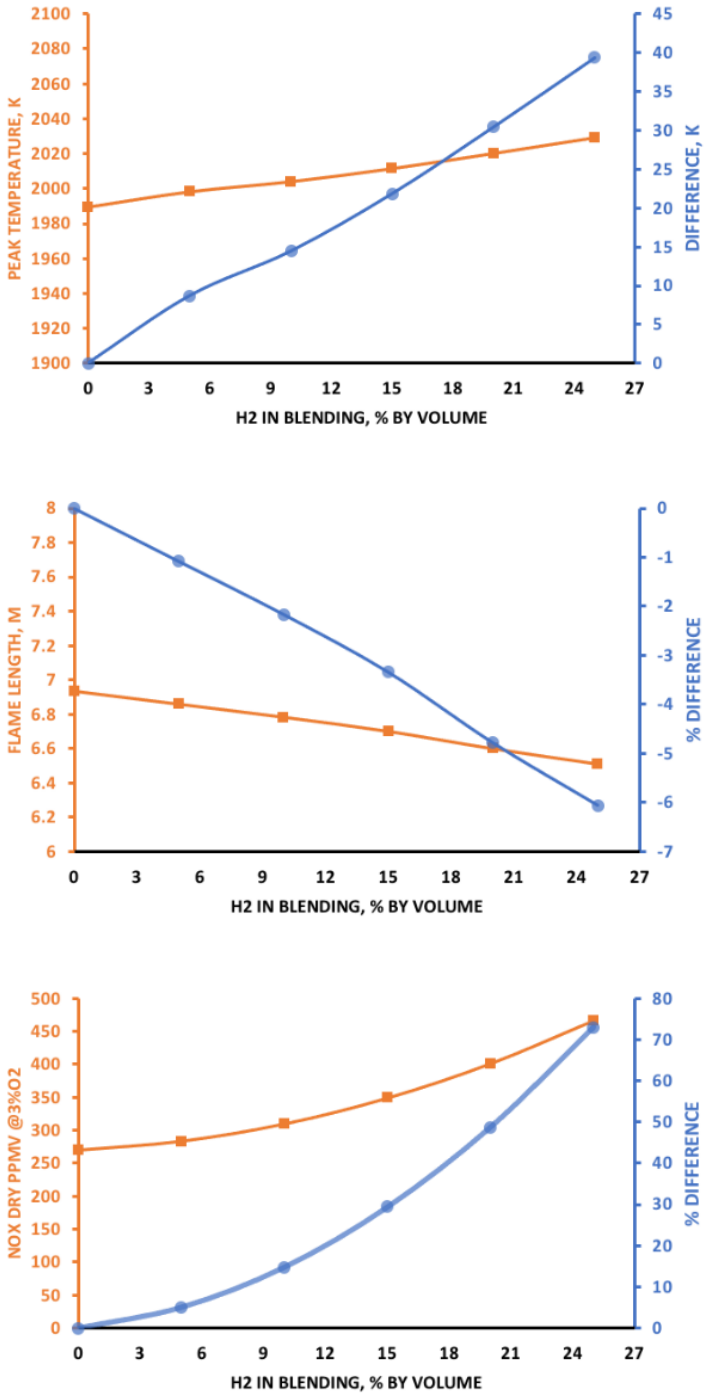

Figure 17: Peak temperature, flame length and NO_x emissions as a function of H_2 blending ratio, for a non-swirled primary air stream (α =10%, λ = 1.3, secondary air temperature = 1000 °C).

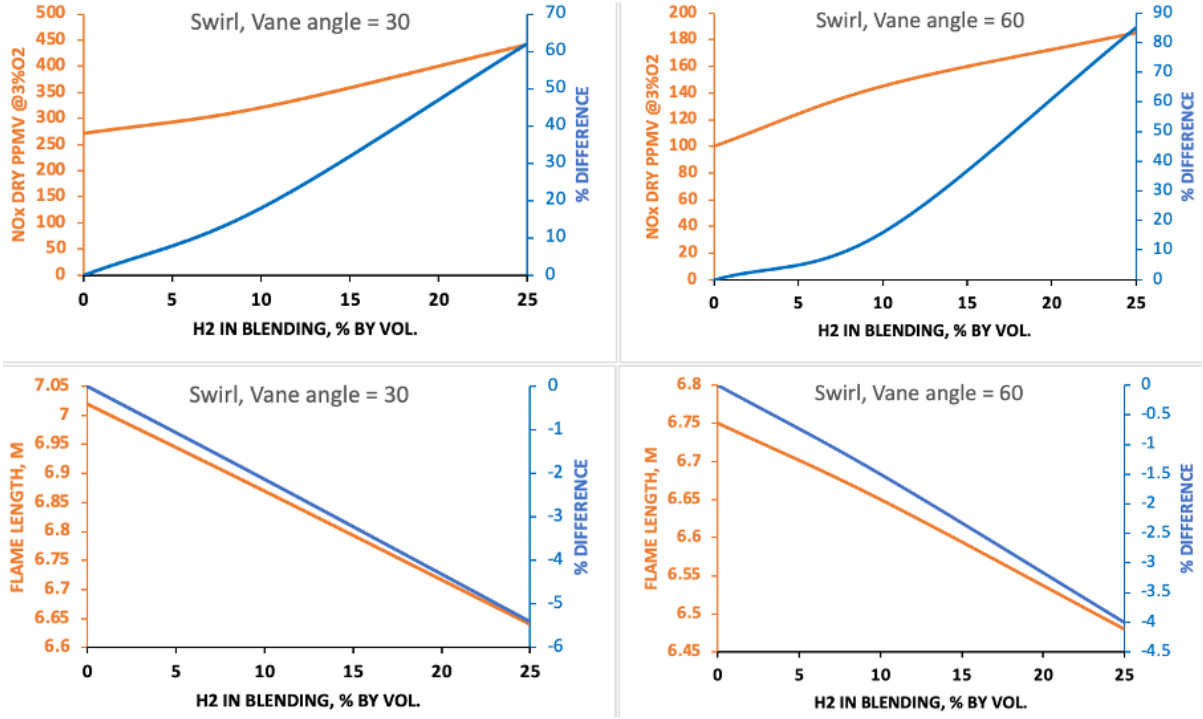

Figure 18: Peak temperature, flame length and NO_x emissions as a function of H_2 blending level, for selected swirled primary air stream cases (α =10%, λ = 1.3, secondary air temperature = 1000 °C).

Various NO_x control strategies have been developed for rotary kilns. In particular, with primary air ratio, α, being a key controlling parameter for NO_x formation. Table 9 reports the impact of decreasing α, from 10 down to 3%, on NO_x emissions for the selected kiln burner design and for a swirl vane angle of 30°. It can be seen that by simply adjusting the value of α, similar NO_x emissions to that of NG-only case can be obtained even for a 25% H_2 blending level. However, it is important to note that, if a NG-fired burner operates without primary air (or with a very low value), other strategies (e.g., staging) will need to be designed and implemented to ensure relatively small changes in NO_x for a 25% H_2 blending level in comparison with NG-only case.

Table 9: Calculated NO_x emissions as a function of fuel type and primary air ratio, for a swirl vane angle of 30°

Fuel	Primary air ratio, α (%)	NO_x @ 3% O_2 (ppmv)	Difference (%)
CH_4	10	272	–
CH_4/H_2, H_2 = 10%	10	321	+18
CH_4/H_2, H_2 = 25%	10	441	+62
CH_4/H_2, H_2 = 10%	3	200	-25
CH_4/H_2, H_2 = 25%	3	292	+7.5

Finally, Figure 19 and Table 10 present, respectively, the axial (total) heat transfer coefficient profile and the variation in the net radiative heat transfer due to H_2 blending, for the case with a swirl vane angle of 30°, α = 10%, and a fixed heat loss at the kiln walls of 0.1 MW (5% of the thermal input). Overall, it can be seen that for all the range of H_2 blending considered here, a negligible variation in the heat transfer characteristics between NG and NG/H_2 were observed, hence suggesting that the performance of the burner would not be affected by H_2 blending up to 25% by volume.

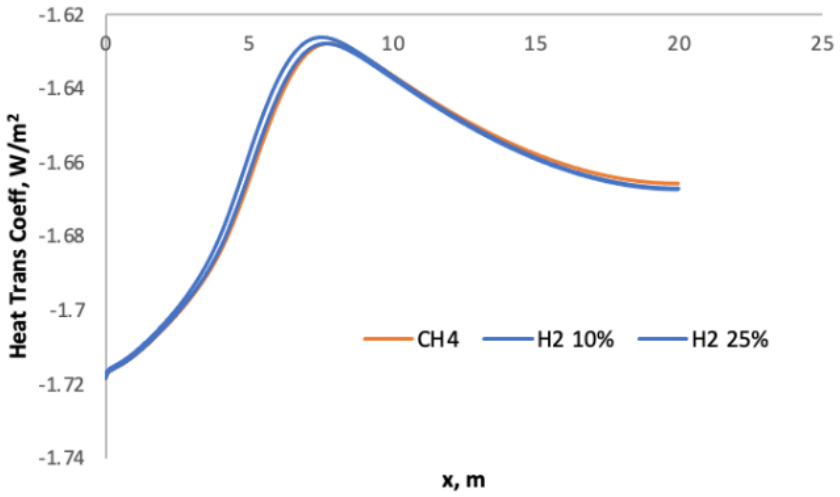

Figure 19: Axial profile of the total heat transfer coefficient as a function of the fuel type, for a swirl vane angle of 30° (α =10%, λ = 1.3, secondary air temperature = 1000 °C).

Table 10: Calculated variation (as %) in the net radiative heat transfer rate as a function of fuel type, and for a swirl vane angle = 30° (α =10%, λ = 1.3, secondary air temperature = 1000 °C)

Fuel	Difference (%)
CH_4	–
CH_4/H_2, H_2 = 10%	-0.24
CH_4/H_2, H_2 = 25%	-0.81

4.2 IRON ORE PELLETISER: MODEL DESCRIPTION AND KEY RESULTS

A preliminary assessment of the impact of H_2 blending on performance of a commercial scale iron pelletiser was also carried out as part of the activities inherent to Milestone 1, noting that after this milestone the scope of the whole program was revised to mainly focus on alumina and integrated cement sector. While a detailed CFD study was performed for a NG-fired kiln, only a limited number of cases were modelled for the iron pelletiser case study. A large-scale FCT downcomer pelletiser system was modelled (6 MW) to preliminary assess the influence of hydrogen blending on flame characteristics and pollutant emissions. The CFD model was developed using the commercial software ANSYS Fluent 2020R2 and was built upon an existing RANS model from industry partner FCT Combustion, employing natural gas as reference fuel and FCT Combustion's I-jet burner design (Figure 20). The model features a 3D unstructured poly-hexcore mesh (approximately 3.5 million cells). The *k*-Ω turbulence closure model was employed for all cases together with a second-order upwind discretization method. The Coupled scheme was used to solve the pressure-velocity coupling. The steady flamelet combustion model was also

employed to solve the chemistry. A reduced GRI-Mech 3.0 kinetic mechanism (contains 325 reactions and 53 species) was used for all simulations (both NG and NG/H_2 cases). The convergence criterion was set to 10^{-6} for all equations. A systematic investigation was carried out by varying the amount of hydrogen blended with NG while fixing all the other parameters (see Table 11 for details of the operating conditions investigated). Note that simulations were performed by varying H_2 % on a mass basis (up to 50% H_2 by mass, corresponding to 88% by volume) for this particular case study.

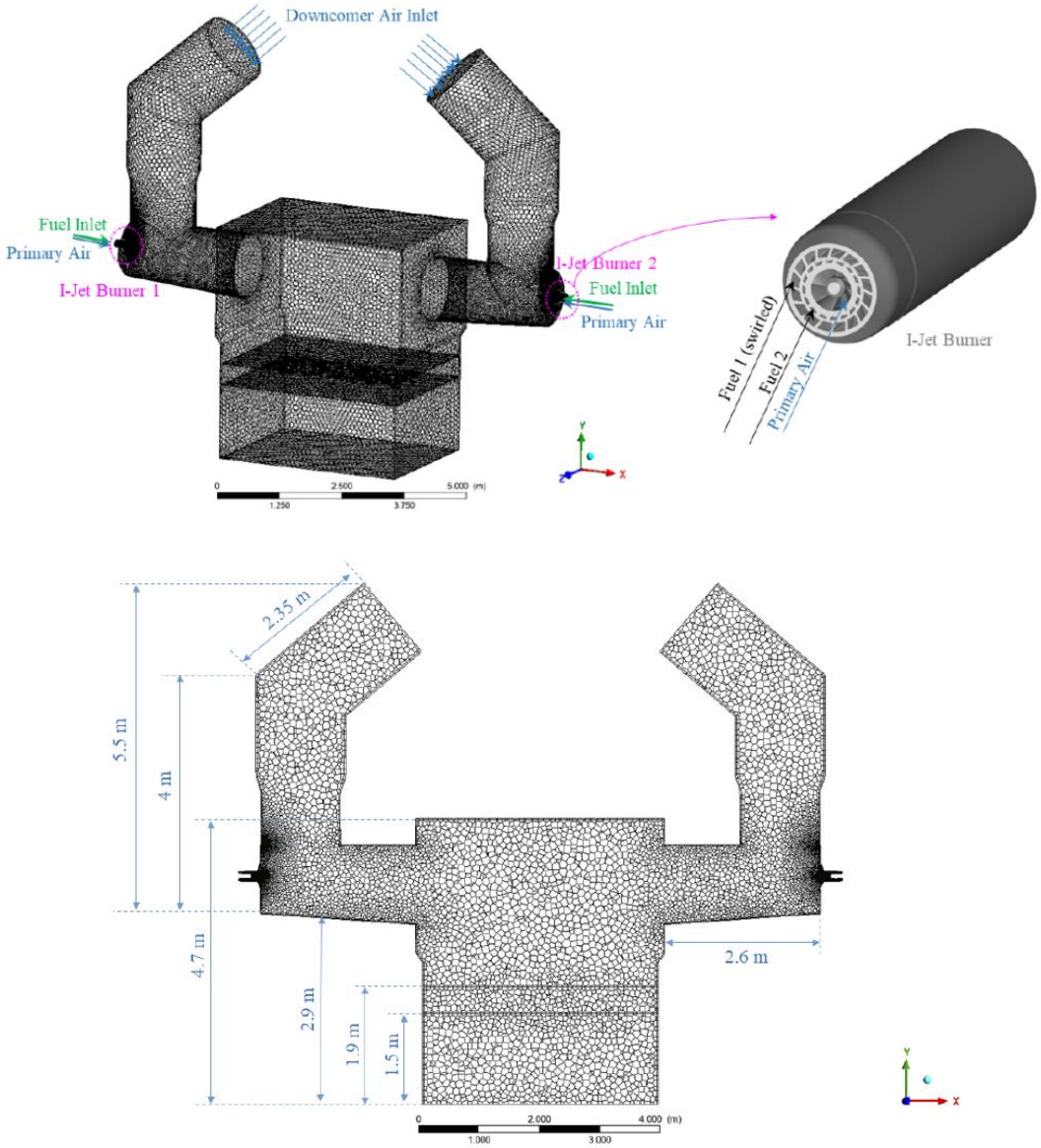

Figure 20: 3D CFD model of a FCT downcomer pelletiser system showing details of the I-jet burner, mesh and geometry size.

Table 11: Operating conditions for the CFD cases investigated. Note that simulations were performed by varying H_2 % on a mass basis for this particular case study.

H_2 % in the fuel stream (by mass)	Power input of each I-jet, MW	Amount of primary combustion air relative to stoichiometry	Downcomer air Temperature, K	Fuel and combustion air temperature, K	Oxidiser composition (by mole)
0	3	10%	1173	300	O_2 = 0.18 N_2 = 0.81 CO_2 = 0.01
10	3	10%	1173	300	O_2 = 0.18 N_2 = 0.81 CO_2 = 0.01
25	3	10%	1173	300	O_2 = 0.18 N_2 = 0.81 CO_2 = 0.01
50	3	10%	1173	300	O_2 = 0.18 N_2 = 0.81 CO_2 = 0.01

Figure 21 presents the temperature and velocity contours at the cross-section plane of the furnace, for all the cases analysed. It can be seen that an increase in H_2 % leads to an increase in the peak flame temperature, and this effect is enhanced for H_2 content higher than 10% by w/w (an addition of 50% by mass of H_2 into the fuel stream led to a 165 K increase in the peak temperature). Nevertheless, the flame morphology and velocity profiles were found to be similar for all cases.

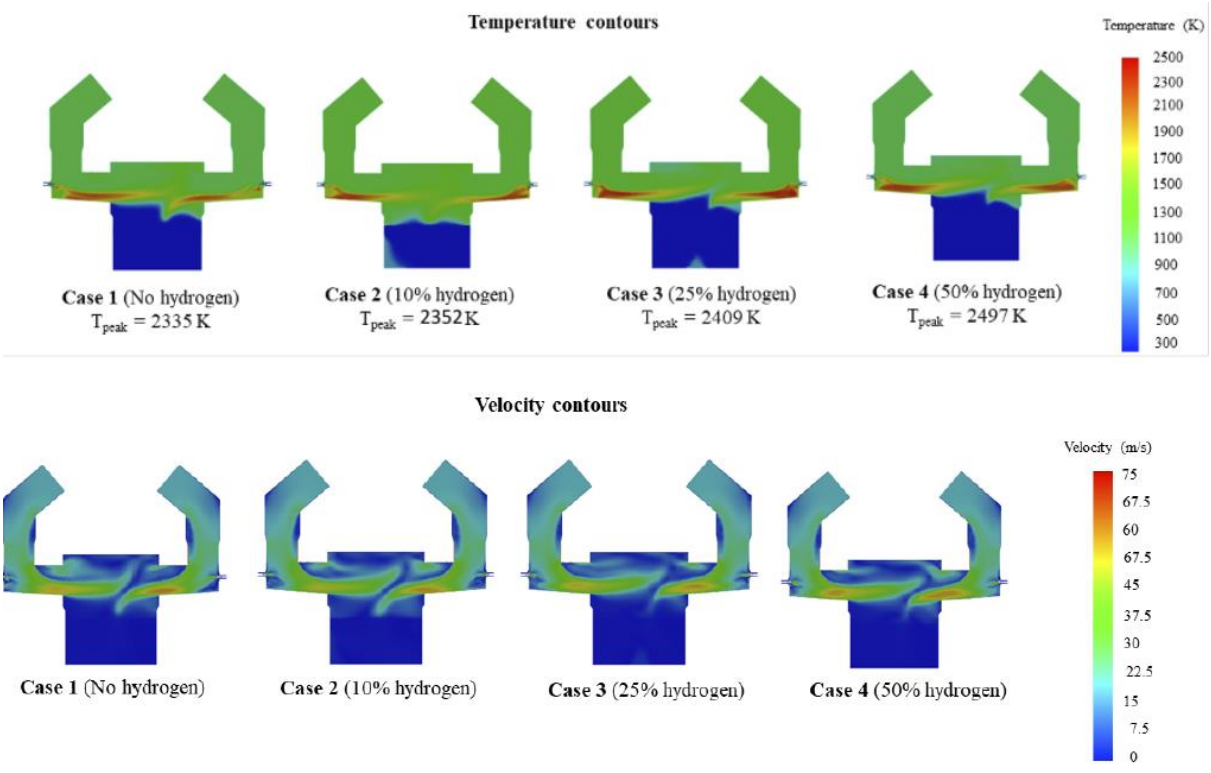

Figure 21: Temperature and velocity contours at the cross-section plane of the FCT downcomer pelletiser system for all the cases investigated (refer Table 11).

Table 12 reports the NO_x emissions and the residual concentrations of key species at the outlet of the device. It can be seen that similar NO_x emissions were found by adding only 10% (by mass) of H_2 to the fuel stream in comparison with NG-only case while up to a 35% increase in NO_x emissions was calculated when adding 50% H_2 (by mass). The amount of residual oxygen was found to be similar for all cases (noting that a value in the order of 16–19% by mole is required to achieve an optimal pelletising process). It was also found that the fuel was completely converted regardless of the initial fuel type.

Table 12: Calculated pollutant emissions and key species at the outlet of the pelletiser system for all the cases investigated.

H_2 % in the fuel stream (by mass)	NO_x dry, ppm @ 3%O_2	O_2 dry, % by mole	CH_4 dry, % by mole	CO dry, % by mole
0	605	16.82	/	$<1e^{-6}$
10	615	16.75	/	$<1e^{-6}$
25	790	16.9	/	$<1e^{-6}$
50	951	16.54	/	$<1e^{-6}$

5. BIO-FUEL DOPING OF H_2-BASED FLAMES

5.1 METHODOLOGY

Bluff-body burners are used to capture the geometric and operating complexities of commercial and industrial burners at lab-scale. Bluff-body burners are useful for their ability to capture the key physics of recirculation and provide increase flame retention and stability, allowing for the study of highly turbulent flames. Two bluff-body burners are used in this investigation to probe the impact of bio-fuel doping as a strategy to enhance the radiation fraction of H_2-based flames, namely a 50-mm and 64-mm diameter bluff-body (d_{BB}) both with a central 4-mm-diameter jet (d_{jet}). An annular contractor with a diameter (d_c) of 190-mm, with honeycomb mesh around the bluff-body burner, delivering uniform co-flow air to the flame. The co-flow velocity is maintained at 11 m/s and 20 m/s for the hydrogen and natural gas/hydrogen flames, respectively. It should be noted that the momentum flux ratio ($\rho_{jet}U_{jet}$:$\rho_{coflow}U_{coflow}$) between these cases varies by no more than 8% across all cases. This ratio has been shown to be the dictating parameter for the vortical structure and the length of the recirculation zone. This burner design has been used previously to study the effects of soot formation in recirculated flow. A diagram of the experimental set up is presented in Figure 22.

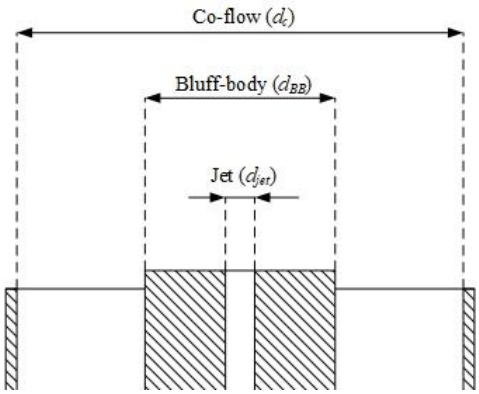

Figure 22: Diagram of the bluff-body burner and annular air contractor arrangement.

Four fuel blends were considered in this investigation: a base NG case, a 10% and 20% (v/v) H_2 cases, and a pure, 100% H_2 case. Reynolds number is conserved at 10,000 for all cases. Pre-vapourised toluene is added at 1–5% (mol/mol) to each fuel blend. Toluene is used as a representative of other bio-oils as it is reported to yield the highest sooting propensity. A DSLR camera and Lux meter are used to compare the visibility of each flame case. Radiant heat transfer is measured using a standard heat flux sensor.

5.2 KEY RESULTS

Figure 23 presents the effect H_2 addition and toluene doping on flame appearance and visibility. Overall, H_2 addition up to 20 vol% in NG flames had a negligible effect on flame appearance and illuminance without the addition of toluene. A stronger contrast is observed between the reference NG and 100 vol% H_2 flame cases. In this case, the 100 vol% H_2 flames were significantly less visible than the reference NG flames. Illuminance results show the pure H_2 was 40 times less luminous than the NG for the 64-mm bluff-body. The addition of toluene had a strong and immediate effect on flame visibility. Toluene addition to the 10% and 20% H_2 cases improved illuminance by up to 10-fold. To achieve a similar illuminance of NG-only, 2–3 mol% toluene with pure H_2 is required.

Split photographs of toluene addition (1–5 mol%) to the 50-mm and 64-mm bluff-body flames and measured illuminance is presented in Figures 23 and 24, respectively. It should be noted that all images presented in this section are photographed through a 594-nm (23-nm full-width at half maximum) notch filter. This is to eliminate the orange colour caused by atmospheric sodium which is an uncontrolled variable that affects how the flames are perceived. The detection orange light emission from H_2 flames due to sodium has been documented in Future Fuels CRC RP1.10-04 Final Report.

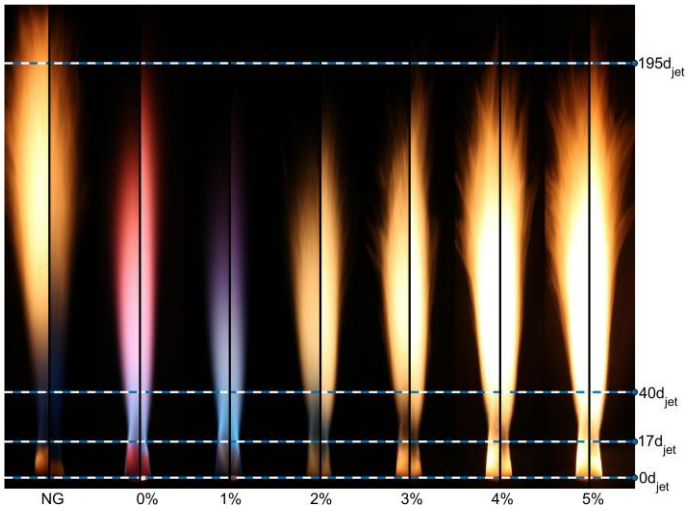

Figure 23: Split photographs of 100 vol% H_2 flames with the addition of 1-5 mol% toluene and stabilised on the 64 mm (left-half) and 50 mm (right-half) bluff-body burner. Reference NG flame photos also included. All flames are operated at Re = 10,000. Aperture and exposure settings from left to right: f/22 2s, f/1.8 4s, f/22 30s, 2s, 1/5s, 1/5s, 1/5s.

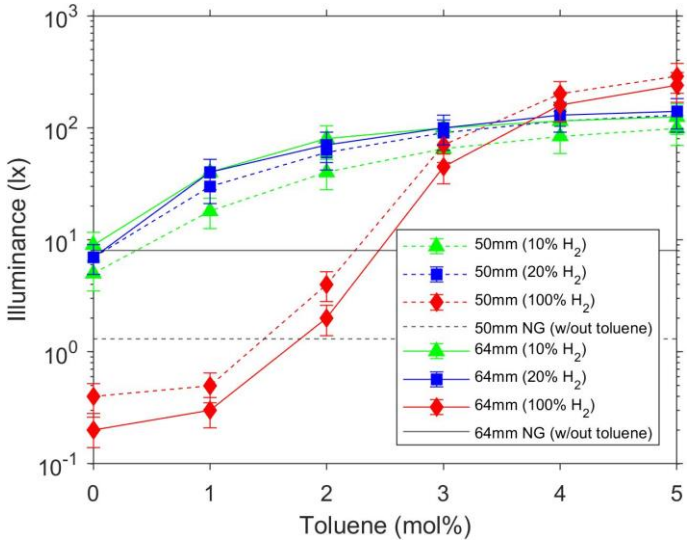

Figure 24: Illuminance (lx) measurements of turbulent pure and blended H_2 in natural gas (NG) (vol%) for the addition of 1-5 mol% toluene, and reference natural gas cases (without toluene addition) in a 50 mm and 64 mm bluff-body burner.

Heat flux measurements for all cases are presented in Figures 25 and 26, for the 50-mm and 64-mm bluff-body burners, respectively. The raw data has been normalised to the heat input of each flame case and is presented per unit area. The normalised heat flux increases with increasing toluene concentration in all cases. No significant reduction in heat flux is recorded for H_2 addition of 10–20 vol% in NG. This suggests that the addition of toluene is not required for these concentrations; however, the heat flux can be significantly improved by the addition of toluene. The 100% H_2 flame had an 80% lower overall heat flux compared to NG with approximately 4 mol% toluene required for the pure H_2 flame to produce a similar heat flux to natural gas. Kinetic analysis of these fuel blends (reported in a journal publication arising from this work [28]) supports the experimental results and suggests the observed changes in heat flux are a result of increased soot formation via the acetylene pathway. The

computational cases also indicated a sensitivity to strain rate in the same way that the experimental cases were sensitive to bluff-body diameter, highlighting the impact that subtle variation in burner design can have on overall performance. It should be noted that the required 4 mol% of toluene, when doped into a pure H_2 flame equates to 65% by mass, and 38% by energy input. This significant contribution of mass and enthalpy from the dopant potentially represent a limitation in the use of toluene as a means of supplementing reduced radiative heat transfer in H_2 flames. This is most likely the cause of the more significant effects of toluene on flame structure and visibility in the pure cases compared with the blended cases, since its contribution to enthalpy and mass by toluene becomes much greater in the 100 vol% hydrogen cases as a result of the increased volumetric flow. From a techno-economic point of view, with an assumption of a NG price of AUD$12/GJ, a bio-oil price of AUD$1.11/L and assuming that the cost of carbon-free H_2 falls to AUD$2/kg, a basic cost analysis was also carried out. With these assumptions, the cost of using H_2 will be AUD$17/GJ compared to AUD$12/GJ for NG, for a given thermal input requirement, i.e., 40% increase in the cost of energy. If bio-oils are to be used with H_2 in the proportions determined by this investigation, the price climbs to AUD$19/GJ, i.e., a 60% increase in the cost of energy. It is also worth noting that, given that the toluene's sooting index is much higher than most bio-oils, this figure is likely to be even higher.

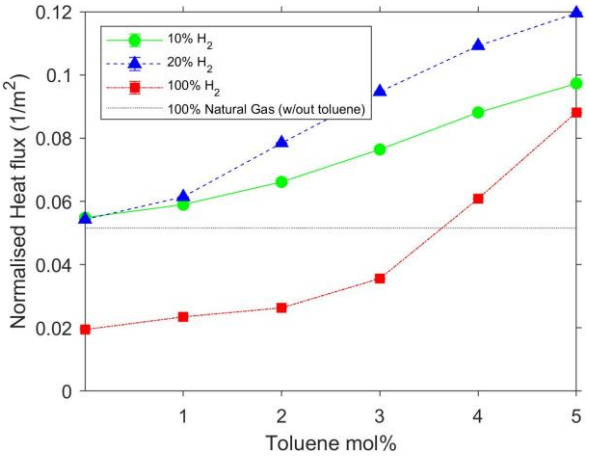

Figure 25: Heat flux data (normalised by heat input) for addition of 1–5 mol% toluene to pure and blended hydrogen/natural gas turbulent flames in a 50 mm bluff-body burner.

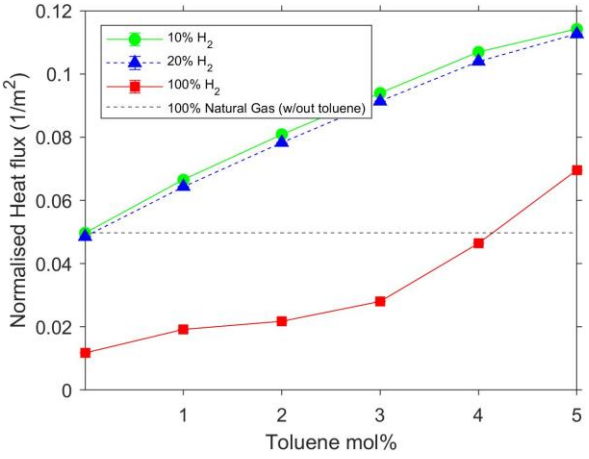

Figure 26: Heat flux data (normalised by heat input) for addition of 1–5 mol% toluene to pure and blended hydrogen/natural gas turbulent flames in a 64 mm bluff-body burner.

6. CONCLUSIONS AND FUTURE WORK

A systematic investigation of the impact of blending hydrogen (H_2) with natural gas (NG) on the Australian alumina and integrated cement sectors was carried out by means of a techno-economic, process and computational fluid dynamics (CFD) analysis, while also probing the efficacy of different adaptation strategies in increasing the radiant fraction from H_2-based flames by means of experimentation.

The joint techno-economic and computational fluid-dynamic analysis of the impact of H_2 blending on the Australian alumina and integrated cement sectors revealed that hydrogen blending has potential to be an effective transition strategy for the decarbonisation of the alumina sector in the short term. For alumina, up to 6% of the current CO_2 sector emissions (corresponding to 1 Mt $CO_{2\text{-}e}$ per year) can be avoided by blending H_2 with NG up to 25% by volume. On the other hand, the carbon emission reduction potential associated with this strategy was found to be weak for integrated cement plants (only 0.39% of the total sector emissions, i.e., 0.02 Mt$CO_{2\text{-}e}$ per year), although there is also unlikely to be any significant penalty for it. The hydrogen parity cost was estimated to be 1–2 A$/kg for a NG price in the range 9–18 A$/GJ. Despite the analysis revealing that an economic gap is still likely to exist between the parity and the predicted H_2 price delivered to the pipeline by 2030 (and also 2050), the impact of H_2 blending on the final cost of commodity was found to be very small (0.01–3% depending on NG and H_2 blending level). The scale of hydrogen needed for hydrogen blending for alumina is also potentially attractive. A requirement of 0.12 Mt of low-carbon H_2 per year would correspond to a 25% blending ratio. This corresponds to half of current Australian H_2 production, making it significant, although this would require new production plant to deliver either blue or green hydrogen. If it were to be produced with green power, it would require 700 MW of electrolysers, making this a very large expansion over current green electrolysers. This shows that the potential demand from alumina producers could be sufficient to drive a step-change in the domestic H_2 consumption, while also achieving a significant total CO_2 mitigation, despite a moderate fractional mitigation of CO_2 emissions.

The process modelling of the last step of the alumina calcination process revealed that switching to blended fuel scenarios with H_2 up to 25% by vol. would represent only a minor technical challenge from a process perspective, with the quality of the produced alumina not expected to vary when the fuel blending ratio is varied, and with key stream temperatures predicted to vary within only 2 Kelvin in comparison with the NG baseline case.

The CFD analysis of a simplified NG-fired rotary kiln burner configuration showed that a relatively small changes will occur to the flame and burner performance when H_2 is introduced into the NG stream, of up to 25% H_2 by volume. Appropriate NO_x control strategies will be needed to avoid an increase in NO_x emissions for the 25% H_2 by volume blend. Similar considerations were found for a straight-grate iron ore pelletiser.

The impact of adding toluene (as representative of a biofuel) as a dopant to 100% H_2 and H_2/NG flames as a strategy to increase both visibility and radiant fraction from flames was also studied and assessed via experiments. The analysis revealed that while this approach can improve both visibility and radiant fraction of H_2-based flames, up to 4% by vol. of toluene would be required for 100% H_2 flame to achieve similar characteristics to that of pure NG flame. This equates to 65% by mass and 40% by energy input, indicating that the amount of doping fuel required is too great for practical use. Also, a basic techno-economic analysis revealed that with current and predicted prices of NG, H_2 and biofuels, this adaptation strategy is very costly, suggesting that alternative strategies should be developed and assessed. To this end, and for successful completion of his PhD, Mr Adam Gee will continue research on H_2 adoption strategies. The focus of his future work will be to experimentally and computationally quantify the effect of H_2 displacement and replacement for several commercial and industrial burners including swirl burners, naturally aerated burners and flame retention burners. This work will also include the assessment of potential strategies such as burner modification and fuel dilution to improve performance of existing burner systems with H_2. Part of Mr Gee's work has also included an assessment of UV emissions from hydrogen flames, which is briefly summarised in Appendix A. The completion of his PhD will contribute to de-risking the adoption of H_2 by industry while providing valuable insight into how existing burners can be sensibly modified to accommodate different fractions of H_2.

7. IMPLICATIONS AND RECOMMENDATION FOR INDUSTRY

This project indicates that H_2 blending is an effective decarbonisation tool for the Australian alumina sector in the short term, offering moderate carbon emissions reduction, negligible increase in the final alumina prices while potentially supporting the establishment of a domestic H_2 supply chain. The process analysis of the last step of the alumina Bayer process highlighted that this step can be undertaken with hydrogen blends (up to 25% by volume) with negligible changes on product quality and process performance, and with no modification to current operations and plant layout needed (other than changes to plant equipment to accommodate H_2 in the valves and flowmeters). Therefore, it is recommended to establish mechanisms supporting communication of these results (from a business case perspective) between the NG producers/operators and the alumina producers to fast-track the adaptation of an H_2 blending strategy in Australia. Nevertheless, the combustion performance (e.g., NO_x emissions, efficiency, fuel flexibility, radiation characteristics) of the burners presently used to provide the heat input into alumina calciners and boilers should be assessed/checked to ensure that these also remain unchanged in comparison with conventional operations. Detailed combustion performance analysis of alumina calciners (and other relevant burners/appliances to the alumina sector) via CFD should be performed, which was not part of the scope of work, but it could potentially be included in a proposal for future activities within the Future Fuels CRC. Discussions with the integrated cement sector should also occur to communicate the key outcomes of the analysis, particularly to highlight how the resilience in heavily utilisation of coal not only lead to high CO_2 emissions but also inhibits the efficacy of transition decarbonisation strategy such as H_2 blending with NG. In addition, the literature review carried out to support the development of a CFD model of a NG-fired rotary kiln highlighted that limited data is available. Access to high quality, quantitative data is paramount to support the development and validation of predictive models. Therefore, it is also recommended to develop mechanisms supporting the establishment of a dedicated combustion facility (of appropriate scale, e.g. 1 MW) in Australia to be able to generate unique hydrogen-based datasets relevant to a series of industrial scale processes/burners. Finally, it is recommended to explore alternative strategies to that of biofuel doping in H_2-based flames as a means to increase visibility and/or radiant fraction. This because of the very high cost associated with this approach as well as with the much higher share of the total energy input of the dopant fuel in comparison with that of H_2 (so that H_2 would be considered “dopant” to some extent). One potential approach, which will be investigated by Mr Adam Gee in the remaining of his PhD activities, will be around actual burner modification and fuel dilution to improve performance of existing burner systems.

8. REFERENCES

[1] https://www.energy.gov.au/sites/default/files/Australian%20Energy%20Statistics%202022%20Energy%20Update%20Report.pdf

[2] Department of Industry, Science, Energy and Resources 2021. Resources and Energy Quarterly: September 2021. https://www.industry.gov.au/data-and-publications/resources-and-energy-quarterly-2021

[3] Australian Aluminium Council Report 2020. https://aluminium.org.au/sustainability/

[4] D Thurtell 2021. Resources and Energy Quarterly 2021.

[5] Ministers for the Department of Industry, Science, Energy and Resources. Supporting a low emissions future in alumina refining. https://www.minister.industry.gov.au/ministers/taylor/media-releases/supporting-low-emissions-future-alumina-refining

[6] Department of Industry, Science, Energy and Resources 2021. Australia's National Hydrogen Strategy. https://www.industry.gov.au/data-and-publications/australias-national-hydrogen-strategy

[7] Australian Cement Report 2020. http://cement.org.au/wp-content/uploads/2020/08/CIF-Industry-Report-2020.pdf

[8] I Yilmaz and M Ilbas 2008. An experimental study on hydrogen-methane mixture fuels. International Communications in Heat and Mass Transfer. 35 (2), 178-187

[9] Kar, S.K., Sinha, A.S.K., Bansal, R., Shabani, B. and Harichandan, S., Overview of hydrogen economy in Australia. WIREs Energy and Environment. n/a(n/a): p. e457 DOI: https://doi.org/10.1002/wene.457.

[10] Milani, D., Kiani, A. and McNaughton, R., Renewable-powered hydrogen economy from Australia's perspective. International Journal of Hydrogen Energy, 2020. 45(46): p. 24125-24145.

[11] Australia's National Hydrogen Strategy, in Council of Australian Governments (COAG) Energy Council. 2019, Department of Industry, Science and Energy Resources: Canberra.

[12] A Chinnici et al. (2022). Future Fuels CRC 1.4.03 Milestone 4 Report

[13] Advisian Worley Group 2021. Australian hydrogen market study. Sector analysis summary.

[14] Alumina Limited 2020 Half Year Report. https://www.aluminalimited.com/database-files/view-file/?id=17491

[15] Boral 2020 Half Year Report. https://www.boral.com/sites/corporate/files/media/field_document/1H20-Results-Presentation.pdf

[16] IEA Special Report 2021. The role of low-carbon fuels in the clean energy transitions of the power sector. https://www.iea.org/reports/the-role-of-low-carbon-fuels-in-the-clean-energy-transitions-of-the-power-sector?utm_content=buffer19fb2&utm_medium=social&utm_source=linkedin.com&utm_campaign=buffer

[17] Deloitte 2019. Australian and global hydrogen demand growth scenario analysis. https://www2.deloitte.com/content/dam/Deloitte/au/Documents/future-of-cities/deloitte-au-australian-global-hydrogen-demand-growth-scenario-analysis-091219.pdf

[18] Grattan Institute 2010. Restructuring the Australian economy to emit less carbon: detailed analysis

[19] Department of Industry, Science, Energy and Resources. Resources and Energy Quarterly: December 2020. https://publications.industry.gov.au/publications/resourcesandenergyquarterlydecember2020/documents/Resources-and-Energy-Quarterly-Dec-2020-Aluminium.pdf

[20] E Elattar et al. 2016. CFD modelling using pdf approach for investigating the flame length in rotary kilns. Heat Mass Transfer 52, 2635-2648

[21] E Elattar et al. 2020. Swirled jet flame simulation and flow visualisation inside rotary kiln-CFD with pdf approach. Processes 8, 159

[22] E Elattar et al 2016. Study of parameters influencing fluid flow and wall hot spots in rotary kilns using CFD. Can. J. Chem. Eng. 94, 355-367

[23] A Chinnici et al 2018. Combined solar energy and combustion of hydrogen-based fuels under MILD conditions. Int. J. Hydrogen Energy 43, 20086-20100

[24] A Chinnici et al 2017. Comparison of system performance in a hybrid solar receiver combustor operating with MILD and conventional combustion. Part I: solar-only and combustion-only employing conventional combustion. Solar Energy 147, 489-503

[25] A Chinnici et al 2017. Comparison of system performance in a hybrid solar receiver combustor operating with MILD and conventional combustion. Part II: Effect of the combustion mode. Solar Energy 147, 479-488

[26] JJ Parham et al 2000. The relationship between heat flux and NO_x emissions in gas-fired rotary kilns. Journal of the Energy Institute

[27] Ilbas et al 2005. Investigations of hydrogen and hydrogen-hydrocarbon composite fuel combustion and NOx emissions characteristics in a model combustor. Int. J. Hydrogen Energy 30, 1139-1147

[28] A Gee et al 2022. Toluene addition to turbulent H2/natural gas flames in bluff-body burners. Int. J. Hydrogen Energy 30, 27733-37746.

APPENDIX A – UV EMISSIONS

A.1 BACKGROUND

Some members of the Future Fuels CRC community raised possible concern that the well-known increase in UV emissions from hydrogen flames, primarily as a result of the increase OH* production, may pose a risk for applications where skin exposure is likely. Some experiments were conducted as initial scoping tests to determine if this concern warrants a more detailed investigation and project proposal.

A.2 METHODS

The burner used for this testing is a partially premixed self-aspirating pizza oven burner shared with Future Fuels CRC project RP1.4-08. The burner features an adjustable venturi valve and flame retention nozzle. The default burner management system was removed from the burner for this testing to isolate the burner from the pilot flame and avoid unintentional shut off due to the flame rectification failing on large fractions of hydrogen. Two flames are considered: a partially premixed natural gas flame with the venturi set to allow maximum air flow and a non-premixed hydrogen flame. Both fuels are supplied at 35 kW using Alicat mass flow controllers.

Flame spectra data is detected with a Red Tide USB650UV spectrometer (over the range 200–400nm) and collected with a Thorlabs SM1CP1 UV mirrored collimator. An integration time of 1500 ms is chosen to provide adequate signal-to-noise ratio. The spectrometer sensor is positioned 100 mm above the burner and 500 mm radially from the flame centreline.

For comparison, spectrometry data is also taken outside pointed directly at the sun on an overcast day, where sun protection is generally not needed (as classified by the Bureau of Meteorology, UV index 2). For the sake of direct comparison, the same 1500 ms integration time is used as with the flames. In addition to detailed spectra data, an RS-Pro UV-AB (290–390nm) meter is used to compare the UV emissions from the flames with those outside, under the same conditions described above. In this case, the UV meter positioned such that the maximum signal is achieved. It should be noted that the UV meter does not detect radiation in the UV-C band (100–280nm) although the spectrometer does provide coverage down to 200 nm.

A.3 RESULTS –SPECTRA

Flame spectrometry data for a non-premixed hydrogen flame and partially premixed natural gas flame at constant heat input (35kW) is presented in Figure 1. Additionally, for comparison, a spectra measurement of the sun, taken outside on an overcast day is included for reference.

The spectra for both flames is typical with the main peaks identified by the characteristic species in flames. The natural gas flame has the expected CH* chemiluminescence (~430 nm) and C_2 Swan bands (peaking ~515 nm) as well as broadband emissions from nascent soot and soot precursors. The H_2O vapour lines in the red (>700nm) are especially pronounced for the hydrogen flames. Both flames have the atmospheric sodium impurity peak (~589 nm). The OH* signature, with peaks around 285 nm and 310 nm is present in the UV region, corresponding to the A–X (0,0) and (1,0) transitions, respectively. The hydrogen flame generates approximately four times more OH* emissions than the natural gas case. Although there are known transitions at shorter wavelengths within the spectral range of the spectrometer (e.g. ~262 nm and ~245 nm for the A–X (2,0) and (3,0) transitions, respectively) these are below the intensity detection limit.

The spectra line for ‘outside’ is taken at the same integration time as the flames. At this integration time, the higher intensity of light outside exceeds the limit of the sensor. Conversely, when the spectra from outside is correctly exposed, the flame spectra is undetectable. However, for some of the spectral region of interest (<300 nm) the signal from outside is not saturated, as a result of UV-B (280–315 nm) and UV-C (100–280 nm) being significantly filtered by the ozone layer. These results imply a much stronger UV signal from the sun on an overcast day than is emitted from a pure hydrogen flame.

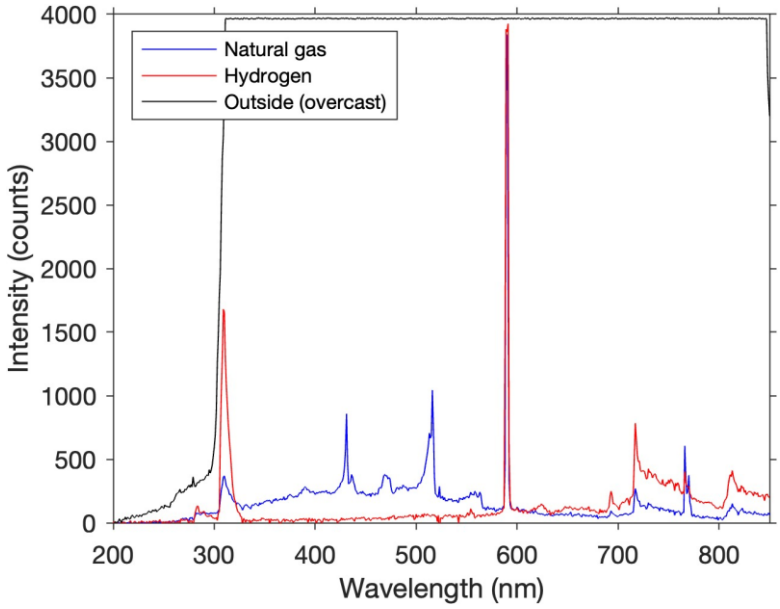

Figure 1: Emissions spectra of partially premixed natural gas and diffusion hydrogen flames in a commercial AN venturi burner, both supplied at 35 kW. The spectra emission profile of the sky, taken outside on an overcast day is also presented for comparison. All data was collected with an integration time of 1500 ms and with dark charge signal removed.

A.4 RESULTS – UV EMISSIONS

In addition to the spectrometry results, a UV meter was used to take irradiance measurements of a variety of flames and again compare the results to outdoor conditions.

The results are presented in Table 1. The UV meter has a resolution of 1 μW/cm^2. No signal was detected when pointed at any of the flames tested. Various heights, distances and angles were tested and for all cases no signal could be measured. When the sensor was taken outside on an overcast day the sensor read ~1000μW/cm^2.

Extracting UV-index information from simple irradiance measurements is challenging, however, given a sensor reading of <1 μW/cm^2 from the flames, compared with ~1000μW/cm^2 on a cloudy day where skin protection is not considered necessary, implies that trying to determine the UV-index from the flames is not necessary.

Table 1: UV irradiance of hydrogen and natural gas flames with various degrees of premixing, data is also presented of the sky, taken outside on an overcast day.

Case	**UV-meter reading (μW/cm²)**
Inside lab (lights on, windows open)	<1
Outside (overcast day)	~1000
Natural gas (35k) venturi fully open	<1
Natural gas (35kW) venturi closed	<1
Natural gas (35kW) venturi partially open	<1
Hydrogen (35kW) venturi closed	<1
Hydrogen (35kW) venturi partially open	<1

A.5 CONCLUSIONS

The initial scoping results from flame spectrometry and irradiance measurements indicate that UV emissions from hydrogen flames are moderately higher than from natural gas flames, but still orders of magnitude less than the UV outside on an overcast day, where sun protection is generally not needed. On this basis, while hydrogen does emit a greater amount of radiation in the UV region compared with natural gas flames, this does not appear to be significant from a human skin exposure standpoint.

It should be noted that the results presented in Appendix A are from a 35 kW burner only. A series of tests were also performed on smaller Type A domestic cookers. Although the results were not recorded, the observed trends were consistent with those from the 35 kW flames: namely the spectra showed the same features and the measurements on the UV meter were indistinguishable above the background. It is possible that flames larger than 35 kW may emit greater levels of UV radiation. Although humans are less likely to be exposed to such flames, further consideration may be warranted in those scenarios.

THIS PAGE SHOULD BE LEFT BLANK

Future Fuels CRC

Enabling the Decarbonisation of Australia's Energy Networks

www.futurefuelscrc.com

info@futurefuelscrc.com

Australian Government
Department of Industry, Science, Energy and Resources

Business Cooperative Research Centres Program